Hemispherically asymmetric trade wind changes as signatures of past ITCZ shifts

David McGee[a,1], Eduardo Moreno-Chamarro[a], Brian Green[a], John Marshall[a], Eric Galbraith[b,c], Louisa Bradtmiller[d]

5   [a] Department of Earth, Atmospheric and Planetary Sciences, Massachusetts Institute of Technology, Cambridge, MA USA; davidmcg@mit.edu; chamarro@mit.edu; brianmg@mit.edu; jmarsh@mit.edu

[b] Institut de Ciència i Tecnologia Ambientals (ICTA) and Department of Mathematics, Universitat Autonoma de Barcelona, Spain; eric.d.galbraith@gmail.com

10   [c] ICREA, Barcelona, Spain

[d] Department of Environmental Studies, Macalester College, Saint Paul, MN USA; lbradtmi@macalester.edu

[1]Corresponding author: davidmcg@mit.edu

Abstract: Paleo-reconstructions of the Intertropical Convergence Zone (ITCZ) and Hadley cells provide important evidence of how atmospheric circulation, tropical precipitation patterns, and interhemispheric asymmetries can change in response to climate perturbations. While most such reconstructions have focused on ITCZ-related rainfall, here we show that trade wind proxies can document dynamical aspects of meridional ITCZ shifts. Theoretical expectations based on angular momentum constraints and results from freshwater hosing simulations with two different climate models predict that ITCZ shifts due to anomalous cooling of one hemisphere would be accompanied by a strengthening of the Hadley cell and trade winds in the colder hemisphere, with an opposite response in the warmer hemisphere. This expectation of hemispherically asymmetric trade wind changes is confirmed by proxy data of coastal upwelling and windblown dust from the Atlantic basin during Heinrich stadials, showing trade wind strengthening in the Northern Hemisphere and weakening in the Southern Hemisphere subtropics in concert with southward ITCZ shifts. Data from other basins show broadly similar patterns, though improved constraints on past trade wind changes are needed outside the Atlantic Basin. The asymmetric trade wind changes identified here suggest that ITCZ shifts are also marked by intensification of the ocean's wind-driven subtropical cells in the cooler hemisphere and a weakening in the warmer hemisphere, which induces cross-equatorial oceanic heat transport into the colder hemisphere. This response would be expected to prevent extreme meridional ITCZ shifts in response to asymmetric heating or cooling. Understanding trade wind changes and their coupling to cross-equatorial ocean cells is key to better constraining ITCZ shifts and ocean and atmosphere dynamical changes in the past, especially for regions and time periods for which few paleodata exist.

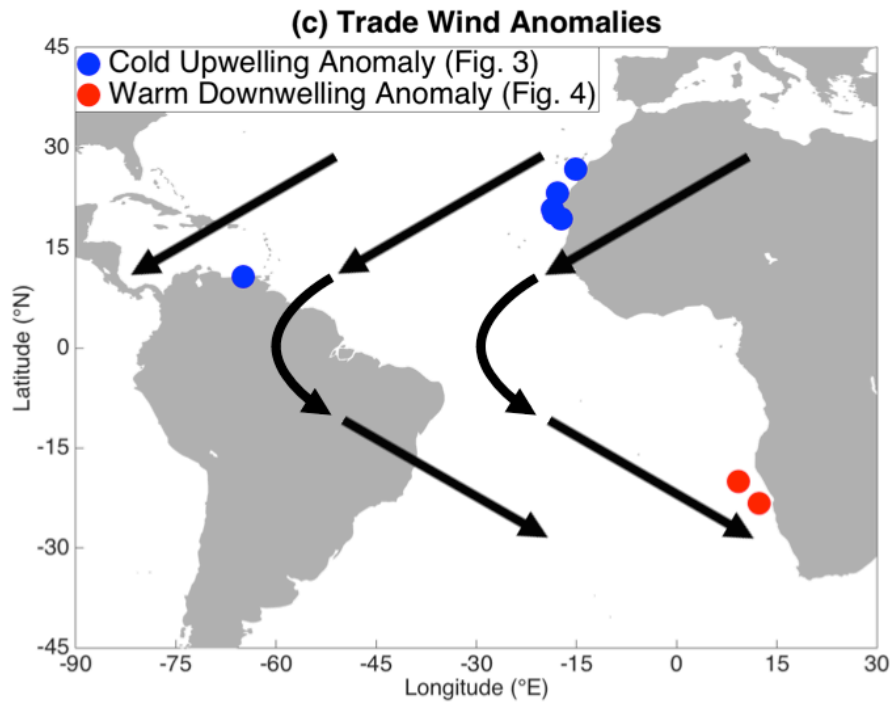**Keywords:** ITCZ; tropics; Heinrich stadials; Quaternary; climate dynamics; global
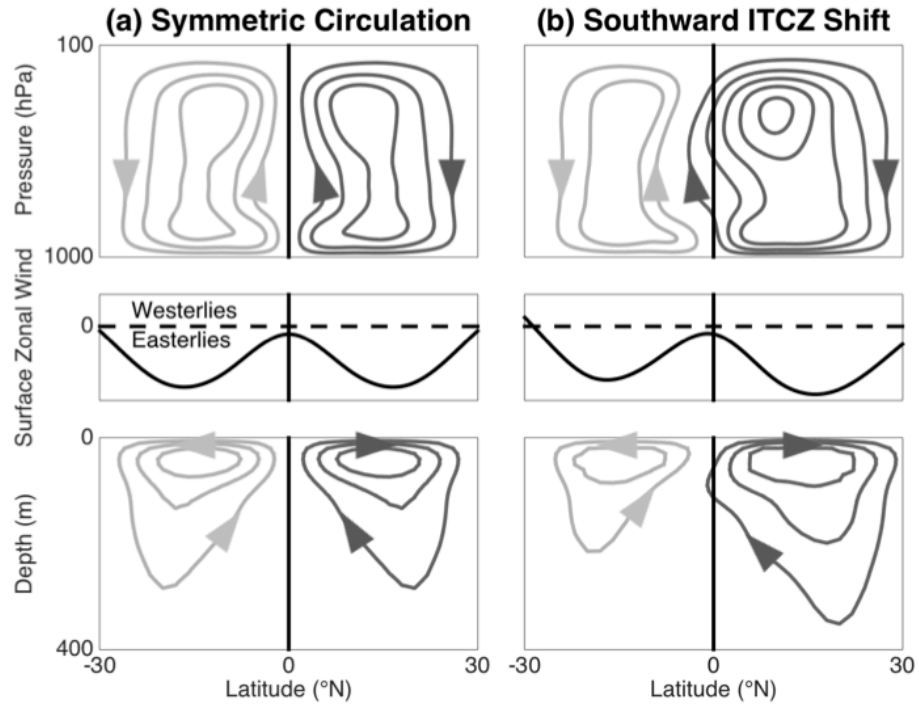
1. Introduction

The paleoclimate record contains abundant evidence of past perturbations of the balance of surface temperatures between the two hemispheres, and as such it provides unique insights into the climate system's response to hemispherically asymmetric heating (Broecker and Putnam, 2013; Schneider et al., 2014). The clearest examples of such perturbations are millennial-scale coolings of the Northern Hemisphere (stadials) that occurred during the last glacial period (Dansgaard et al., 1982; Alley et al., 1993; Bond et al., 1993; Taylor et al., 1993; Blunier et al., 1998; Blunier and Brook, 2001; EPICA Community Members, 2006; Clement and Peterson, 2008). During these events, expansions of sea ice in the North Atlantic and reduction of cross-equatorial ocean heat transport associated with the Atlantic Meridional Overturning Circulation (AMOC) are thought to have cooled the Northern Hemisphere (NH) (Boyle and Keigwin, 1987; Clement and Peterson, 2008; Henry et al., 2016; Li et al., 2005) and warmed the Southern Hemisphere (SH) (Barker et al., 2009; Blunier et al., 1998; Broecker, 1998; Buizert et al., 2015). The most prolonged of these stadials were also marked by iceberg discharge into the North Atlantic and are known as Heinrich stadials (Hemming, 2004). Stadials have been connected with shifts in the tropical rain belt associated with the Intertropical Convergence Zone (ITCZ) and changes in monsoon strength. A broad range of evidence indicates a southward shift of the ITCZ, a weakening of NH monsoons, and a strengthening of at least the South American summer monsoon in the SH in response to NH cooling (Arbuszewski et al., 2013; Baker, 2001; Collins et al., 2013; McGee et al., 2014; Peterson, 2000; Placzek et al., 2006; Wang et al., 2007, 2004; Wang, 2001).

A variety of modeling experiments have found a qualitatively similar southward shift of the ITCZ in response to NH cooling. In these studies, ITCZ shifts are accompanied by a

60   pronounced intensification of the annual-mean Hadley cell in the NH and a weakening in the SH, with each hemisphere's trade winds – the surface expression of the Hadley circulation – changing in kind (Figures 1 and 2) (Broccoli et al., 2006; Chiang, 2003; Chiang and Bitz, 2005; Dahl et al., 2005; Timmermann et al., 2005; Vellinga and Wood, 2002; Zhang and Delworth, 2005). As we review below, this asymmetric Hadley cell and trade wind response is a

65   fundamental expectation of the atmosphere's response to asymmetric cooling of one hemisphere and a shift of the ITCZ toward the warmer hemisphere.

      Trade wind changes are central to the dynamics of stadials and other perturbations of interhemispheric temperature differences. By regulating upwelling along eastern boundaries, trade winds determine surface productivity and air-sea heat and carbon dioxide fluxes over large

70   areas of the world's oceans. Trade winds also have a pronounced influence on the ocean circulation, helping drive the circulation of the subtropical gyres and subtropical cells. Attempts to model ocean circulation in the Atlantic during the Last Glacial Maximum (LGM) have demonstrated that even small changes in surface trade winds can alter ocean circulation and improve data-model agreement (Amrhein et al., 2015; Dail and Wunsch, 2014); as such, accurate

75   characterization of trade wind responses during stadials may be essential to modeling of the ocean's response to these events. Trade winds modulate evaporative fluxes from subtropical oceans, leading to sea surface temperature (SST) cooling in the hemisphere in which trade winds intensify; this wind-evaporation-SST (WES) feedback may play a central role in communicating high-latitude cooling to the low latitudes (Chiang and Bitz, 2005), and may warm tropical SSTs

80   in the opposite hemisphere, where trade winds are expected to weaken. Perhaps most importantly for the dynamics of abrupt climate change, trade wind-driven intensification of the ocean's subtropical cells may increase ocean heat transport into the cooler hemisphere, limiting the

(a) Symmetric Circulation

(b) Southward ITCZ Shift

Pressure (hPa)

100

1000

Surface Zonal Wind

Westerlies

0

Easterlies

Depth (m)

0

400

-30   0   30
Latitude (°N)

-30   0   30
Latitude (°N)

(c) Trade Wind Anomalies

● Cold Upwelling Anomaly (Fig. 3)
● Warm Downwelling Anomaly (Fig. 4)

45

30

15

Latitude (°N)

0

-15

-30

-45

-90 -75 -60 -45 -30 -15   0   15   30
Longitude (°E)

85 **Figure 1. A-B,** Idealized zonally averaged Hadley circulation (*top*; with dark grey/light grey

describing a clockwise/anticlockwise circulation), surface zonal winds (*center*) between 30ºN

and 30ºS, and zonally averaged subtropical cells (*bottom*, with colors the same as in the top

panel) in (**A**) a hemispherically symmetric scenario and (**B**) an asymmetric scenario of a

southward ITCZ shift. **C.** Anomalies in surface winds (*arrows*) in response to a southward ITCZ

90 shift. Expected changes in sea-surface temperature (SST) and upwelling in response to Heinrich

events are shown at sites in the Atlantic Ocean discussed in the text. Panels A and B adapted

from Green and Marshall (2017).
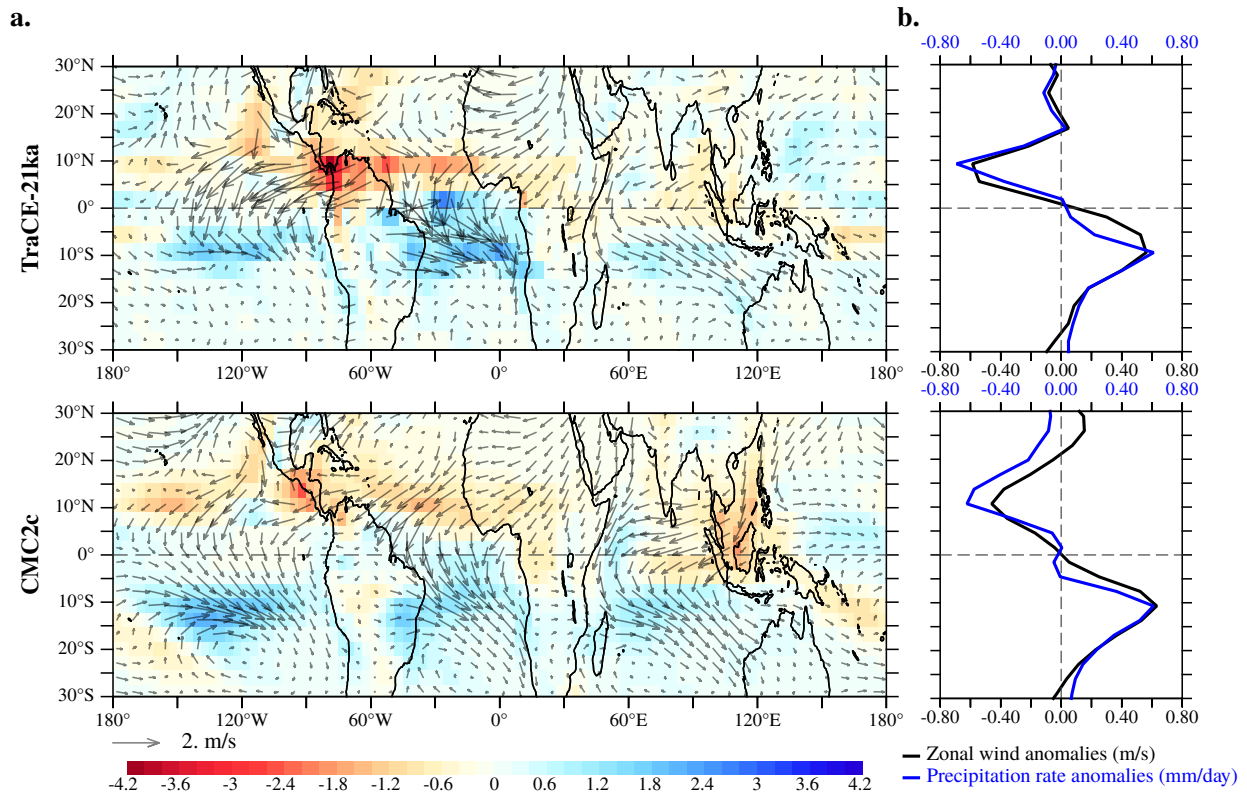
Figure 2. A. Anomalies in annual-mean precipitation rate (in mm/day; *blue-red shading*) and near-surface (10 m) wind (in m/s; *arrows*) between the Heinrich Stadial 1 and the LGM (averaged over the periods 16.5-15.5 ka and 21-20 ka respectively) in the TraCE-21ka simulation (*top*) and between the hosing and their respective control experiments with the CM2Mc model (*bottom*). For the latter case the average of the anomalies of the four experiments is shown. **B.** Anomalies, calculated as in **A**, of the zonally averaged, annual-mean precipitation rate (in mm/day; *blue line*) and near-surface zonal wind (in m/s; *black line*) in the TraCE-21ka simulation (*top*) and on average for the CM2Mc experiments (*bottom*).

105   magnitude of ITCZ shifts (Green and Marshall, 2017; Yang et al., 2017, 2013).

It is thus clear that trade winds are more than passive tracers of atmospheric circulation changes during NH cooling events; rather, they actively modulate the atmosphere-ocean system's response to asymmetric warming/cooling. Reconstructions of trade wind changes during NH cooling events thus have the potential to provide unique insights into the dynamics of

110   the atmosphere and ocean's response to asymmetric warming or cooling. Proxy-based constraints on trade wind changes are particularly valuable in light of models' long-standing biases in simulating the ITCZ (Oueslati and Bellon, 2015), which raise questions about the accuracy of simulated responses to forcing.

Despite this potential, few studies have focused on reconstructing trade wind responses to

115   changes in the balance of heating between the hemispheres. Most observational studies of the tropical atmosphere's response to NH cooling events have employed precipitation proxies (Arbuszewski et al., 2013; Baker, 2001; Collins et al., 2013; Peterson, 2000; Sachs et al., 2009; Schneider et al., 2014; Wang et al., 2004) and have focused on the behavior of the tropical rain belt and monsoons, leaving changes in the broader Hadley circulation relatively unexplored.

120   Previous investigations of trade winds in Late Pleistocene climates have primarily focused on single regions and on glacial-interglacial changes. Studies in the eastern subtropical Atlantic (Sarnthein et al., 1981), the southeastern Atlantic Ocean (Little et al., 1997; Stuut et al., 2002), the southeastern Indian Ocean (Stuut et al., 2014), and the southeastern Pacific Ocean (Saukel, 2011) have concluded that trade winds in each of these regions were more intense during the last

125   glacial period than today, with little indication of hemispheric asymmetry during the last glacial maximum (LGM; ~19-23 ka).

Here we present a compilation of trade wind proxies during Heinrich stadials, the longest and largest-amplitude NH cooling events of the last glacial period and deglaciation, and explore the implications of trade wind changes for the dynamics of these events. This compilation offers an important complement to existing precipitation-based reconstructions, as precipitation proxies are not available everywhere and are particularly sparse over oceans, which underlie the majority of the tropical rain belt. Further, interpretation of precipitation proxies is not always straightforward; each proxy is sensitive to multiple variables, including precipitation amount, evapotranspiration, water vapor source, and convective processes, and the relationship between these variables and the broader Hadley circulation can sometimes be unclear. Trade wind-sensitive proxy data provide additional leverage in testing interpretations of past atmospheric changes, as they directly reflect the tropical atmospheric circulation.

We begin with a description of the dynamics and observations of the trade winds and their response to Northern Hemisphere cooling in models in Section 2. In Section 3, we summarize and evaluate proxies for trade wind intensity. In Section 4, we review evidence for trade wind changes associated with Heinrich stadials and explore the implications of these changes for the Hadley circulation and rain belt. We discuss the implications of these results in Section 5, including the role trade winds play in damping the ITCZ response to interhemispheric temperature differences, and close with a summary of key findings and a discussion of directions for future research in Section 6.

2. Dynamics of wind responses to ITCZ shifts

2.1. Dynamics of the Hadley circulation and trade wind changes accompanying ITCZ shifts

Before describing paleoclimate evidence for trade wind changes during Heinrich stadial events, we provide an introduction to the physical mechanisms underlying the response of the

tropical atmospheric circulation and trade winds to an interhemispheric heating contrast, similar

to the reconstructed conditions during stadials. We start in an idealized state without any heating

contrast between the Northern and Southern hemispheres, nor any cross-equatorial energy

transport. In this idealized configuration, the zonally averaged tropical atmospheric circulation is

155   symmetric about the Equator in the annual mean; the Hadley cells and the surface zonal winds

are of equal strength in both hemispheres (Fig. 1A). The ascending branch of the Hadley

circulation and the ITCZ are therefore situated at the Equator.

        We impose on this symmetric state an interhemispheric heating contrast, with cooling

and warming in the NH and SH extratropics respectively. Such an imbalance is meant to mimic

160   the anomalous heating contrast associated with a shutdown of the AMOC's northward oceanic

heat transport during a Heinrich stadial (e.g., Zhang and Delworth, 2005). Assuming that this

north-south heating contrast is not fully compensated by radiation to space or storage in the

ocean, the atmosphere responds by transporting energy across the Equator to maintain its energy

balance (e.g., Kang et al., 2008). The Hadley cells transport energy in the direction of the air

165   flow within their upper branches, as there is greater moist static energy (the sum of sensible and

latent heat and gravitational potential energy) in their upper branches than in their lower

branches (Neelin and Held, 1987). As a result, a net northward cross-equatorial energy transport

will require an anomalous northward upper-branch flow across the Equator. This is achieved by

shifting the Hadley cells and hence the ITCZ southward, as shown in Fig. 1B. Note that in Fig.

170   1B we also indicate that, along with the southward shift of the system, the NH Hadley cell and

associated trade winds intensify, while the SH Hadley cell and trade winds weaken.

        Hemispherically asymmetric changes in the trade winds can be understood to be a

consequence of the (quasi) conservation of angular momentum. Imagine a ring of air encircling

the globe near the earth's surface along a latitude circle. The rotation of the Earth moves this ring

175   in an eastward direction, termed a 'westerly' velocity. Poleward displacement of that ring

reduces its distance to Earth's axis of rotation, reducing its rotational inertia; if it is to conserve

its angular momentum, it must acquire a westerly velocity. Applying this concept to a southward

shift of the ITCZ and associated trade winds, a near-surface ring of air in the SH that shifts

poleward away from the Equator will contract toward Earth's axis of rotation and acquire a

180   westerly velocity. Conversely, a southward-shifted ring in the NH expands away from the axis of

rotation and acquires an easterly velocity. We therefore expect the trade winds to intensify in the

NH and weaken in the SH, as sketched in Figure 1B. However, the rings' angular momentum is

not perfectly conserved, due to surface friction. The resulting ageostrophic surface wind anomaly

is to the left (right) of the zonal wind anomaly in the NH (SH). This results in a southward

185   (northward) surface trade wind anomaly that strengthens (weakens) the Hadley cell in the NH

(SH), as can be seen comparing Figure 1B to 1A.

A horseshoe pattern of trade wind anomalies emerges when their zonal and meridional

components are combined, as shown schematically for a southward ITCZ shift in the tropical

Atlantic in Figure 1C. These drive anomalous Ekman transports in the surface ocean at right

190   angles to the wind – to the right in the NH and to the left in the SH – which, when combined

with the orientation of the coasts, result in enhanced offshore transport at sites in the NH (blue

dots) and reduced offshore transport at sites in the SH (red dots). Enhanced offshore transport at

NH sites upwells more cool water from depth and SSTs there are reduced, with reduced offshore

transport and upwelling leading to increased SSTs at sites in the SH. Nutrient transport to the

195   photic zone similarly increases in NH upwelling zones and decreases in SH upwelling zones,

driving changes in productivity. Strengthened trade winds are also expected to increase

windblown mineral dust emissions from subtropical dust sources in the NH, while dust emissions

and dust grain size may decrease in the SH subtropics. The physics linking changes in the trade

winds, coastal upwelling, SSTs and mineral dust fluxes to ITCZ shifts allow us to study multiple

200   climate variables when investigating past ITCZ shifts, instead of focusing on changes in

precipitation alone.

2.2. Simulated changes in trade winds during ITCZ southward shifts

Modeling studies of anomalous NH extratropical cooling consistently show southward

205   ITCZ shifts and accompanying changes in the trade winds. Climate models forced with cooling

in the North Atlantic – by imposing a surface freshwater flux there that shuts down the AMOC's

northward oceanic heat transport, for example – show an anomalous atmospheric energy

transport northward across the Equator and a southward ITCZ shift (see the review by Chiang

and Friedman, 2012). Intensified NH trade winds and abated SH trade winds, accompanied by

210   anomalous northerlies at the Equator (similar to Fig. 1C), are most clearly seen in the tropical

Atlantic Ocean in these simulations (Chiang, 2003; Timmermann et al., 2005; Vellinga and

Wood, 2002). Although the same pattern of wind anomalies is not necessarily seen in the other

ocean basins (Timmermann et al., 2005; Vellinga and Wood, 2002), zonally averaged wind

anomalies clearly reflect those in the tropical Atlantic.

215   We complement these previous modeling studies by exploring results from two different

climate model simulations of Heinrich stadials. Both simulations are made with full-complexity

general circulation models, run at roughly 3 degree resolution for the ocean and atmosphere. The

first is the TraCE-21ka simulation, a transient climate simulation of the last 21000 years from the

LGM to the present (Liu et al., 2009). It uses the coupled atmosphere–ocean general circulation

220   model CCSM3, and it is forced with changes in the Earth's orbit, atmospheric CO_2

concentration, ice sheets, sea level, and, during events like Heinrich Stadial 1 or the Younger

Dryas, geologically-informed surface freshwater fluxes via river drainages into the North

Atlantic. The second model 'simulation' is actually the average of four different sets of

freshwater hosing experiments performed with the fully-coupled Earth system model CM2Mc, in

225   which the atmospheric CO_2 concentration, ice sheets, and sea level of the LGM are prescribed

(Brown and Galbraith, 2016). The CM2Mc experiments are run in four different orbital

configurations, reflecting opposite phases of precession and obliquity at its maximum and

minimum values of the last 5 Myr. The orbit's eccentricity is held constant at 0.03. Each orbital

configuration includes a control and a hosed simulation, in which a 0.2 Sv freshwater input is

230   applied uniformly over a rectangular area in the open North Atlantic ocean for 1000 years. The

mean state for each simulation is obtained by averaging the final 100-year-long period of the

1000-year hosing interval. In all cases we show the average of the four orbital configurations.

We focus on changes in the climate between Heinrich Stadial 1 and the LGM in the

TraCE-21ka simulation, and between the hosing experiments and their respective control runs in

235   the CM2Mc model (Fig. 2). These two cases represent a similar scenario in which a shutdown of

the AMOC's northward heat transport induces an anomalous NH cooling. In response to this

cooling, and in agreement with the idealized case discussed in Section 2.1, both models exhibit a

southward ITCZ shift that reduces tropical rainfall in the NH and increases tropical rainfall in the

SH. In the TraCE-21ka simulation, changes in the precipitation rate are most pronounced in the

240   tropical Atlantic, whereas in the CM2Mc experiments the changes are of similar magnitude

across most of the tropical region. Both models thus exhibit a global reorganization of tropical

precipitation, even though the forcing is confined to the Atlantic Ocean. The change in the

13

zonally averaged precipitation rate is strikingly consistent between the models, and reflects a

southward migration in the ITCZ's centroid position (defined following Donohoe et al., 2013) of

245   about 1.2º in the TraCE-21ka simulation, and of about 1.8º on average for the CM2Mc

experiments. Given that these are different models, integrated under significantly different

forcings, this agreement is remarkable. As shown by Brown and Galbraith (2016), the response

of precipitation in CM2Mc to hosing is also quite similar under an interglacial background state,

and is even remarkably similar for unforced internal AMOC oscillations. Drier and wetter

250   conditions develop in the NH and SH tropics respectively, with maximum changes in the zonal

mean precipitation rate around 10ºN and 10ºS in both models.

Changes in the trade winds are also robust across the simulations, with an overall

intensification in the NH and a weakening in the SH (Fig. 2A,B). Regionally, trade wind

anomalies in both models include weakening on the eastern side of all ocean basins in the SH

255   and an intensification in the northern tropical Pacific. In the tropical North Atlantic, by contrast,

changes in the trades slightly differ between the two models: whereas the CM2Mc experiments

show a rather continuous belt of intensified coastal trades along the western African coast, the

TraCE-21ka simulation exhibits a more complex pattern, with anomalous easterlies and

westerlies converging over the eastern tropical North Atlantic and leading to anomalous

260   southerlies along the African coast north of 15ºN. Despite these regional differences, a

hemispherically asymmetric response of the trade winds associated with a southward ITCZ shift

appears as a robust feature in both models (right panels of Fig. 2), and is consistent with the

mechanisms described in Section 2.1. Notably, this consistency occurs despite a significant and

hemispherically-asymmetric change in the global energy balance in the hosing simulations

265   (Galbraith et al., 2016), a change that we ignored in Section 2.1, suggesting that the critical

mechanisms are not affected by the magnitude of energy balance changes that occur. We therefore expect similar changes in proxies of trade wind strength and precipitation intensity during Heinrich stadials.

270 **2.3 Response of low-latitude ocean circulation to trade wind changes**

The low-latitude ocean circulation is primarily driven by the trade winds. Zonal wind stress from the trade winds drives poleward Ekman transport of shallow tropical waters in both hemispheres; these water masses converge and subduct in the subtropics at approximately 30˚ latitude. Subducted water flows equatorward in the thermocline at ~300-400 m depth, upwelling

275 at the equator to close the meridionally overturning subtropical cells (STCs) (Figure 1A, bottom panel) (McCreary and Lu, 1994). Water in the upper limb of the STCs loses heat to the atmosphere as it moves poleward and sinks, leading to a strong temperature gradient between the upper and lower limbs of the STCs. As a result, the STCs are the ocean's primary means of transporting heat from the tropics to the subtropics and closely mirror the atmosphere's Hadley

280 cells (Held, 2001; Klinger and Marotzke, 2000; Trenberth and Caron, 2001).

The direct relationships between the Hadley cells, trade winds, and STC strength in each hemisphere imply that hemispherically asymmetric trade wind changes accompanying Hadley cell shifts will drive similarly asymmetric changes in STC strength. As shown by Green and Marshall (2017), this response results in cross-equatorial flow of warm surface waters into the

285 cooler hemisphere due to relative strengthening of the cooler hemisphere's trade winds and STCs. The anomalous cross-equatorial STC circulation thus transports heat into the cooler hemisphere, partially offsetting the inter-hemispheric heating contrast and damping the atmosphere's response. We explore the implications of this point for ITCZ shifts in Section 5.

3. Trade wind proxies

290   Changes in past trade wind intensity are most often reconstructed using marine sediment records of upwelling and windblown dust. Dust fluxes respond sensitively to changes in surface wind speed, as dust emissions increase at a factor of roughly the cube of the wind speed once a threshold speed is reached (Gillette, 1974; McGee et al., 2010). Dust grain size (either the modal size or the proportion of grains greater than a given size) is expected to increase with increased

295   wind speed (Rea, 1994; Stuut et al., 2002). Sand dune activity is also strongly influenced by wind speed (Roskin et al., 2011; Tsoar, 2005), so reconstructions of dune field activity in trade wind regions can also provide insight into past wind intensity.

However, dust fluxes, grain size and dune activity are each subject to additional controls beyond mean wind speed. Dust flux and dune activity can vary with source aridity, and both flux

300   and grain size are expected to increase if the distance to the source decreases, for example due to exposure of continental shelves in response to falling sea level. The grain size of dust deposited at downwind sites can also change due to changes in dust source area properties (such as the proportion of coarse grains) (Grini and Zender, 2004), changes in the balance of dry deposition (settling) vs. deposition by precipitation scavenging, and changes in transporting winds rather

305   than source area winds. In addition, dust-related proxies reflect dust storms and thus tell us about a long-term mean of high-wind-speed events rather than directly reflecting mean trade wind speed. Nevertheless, it is likely that strong wind events increase with mean trade wind speed, based on the common observation that wind speed variance (and thus the occurrence of strong winds) increases with increasing mean wind speed (Grini and Zender, 2004; Wang et al., 2015).

310   Coastal upwelling also responds sensitively to changes in surface trade winds when the relative orientation of winds and coastlines causes Ekman transport to move surface waters

offshore. In this case, which most commonly occurs along eastern boundaries of subtropical oceans, strengthening of trade winds leads to cooler SSTs and an increased supply of nutrients to the photic zone. These nutrients increase primary productivity and alter species distributions in

315 surface waters, and respiration of sinking organic matter causes dissolved oxygen levels to drop in intermediate-depth waters. As a result, records of the accumulation rate of biogenic sediments (e.g., organic carbon, biogenic opal), species distributions, SSTs and the oxygenation of intermediate-depth bottom waters in upwelling zones have been interpreted to reflect past changes in upwelling intensity (that is, vertical velocities in upwelling zones).

320 However, each of these indicators is controlled by additional factors beyond trade wind speed. Changes in biogenic sediment flux may also reflect changes in the nutrient content of upwelled water (Takesue et al., 2004) or in preservation efficiency in sediments rather than upwelling intensity. Changes in sea surface temperature (SST) may result from changes in the temperature of upwelled waters or surface-advected waters without changes in upwelling

325 intensity. Species distributions may also change due to changes in the temperature and/or nutrient content of upwelled waters. Subsurface oxygenation can change due to changes in the oxygen content of waters entering the upwelling zone rather than oxygen demand. Finally, coastal upwelling intensity is sensitive not just to trade wind speeds but also to wind orientation, as only the coast-parallel component of surface winds drives offshore transport of waters and

330 alongshore upwelling. In places such as the Arabian Sea, the orientation of the coastline leads to anomalous downwelling rather than upwelling in response to strengthened trade winds, producing reduced productivity, increased sub-surface water temperatures, and increased water column oxygenation when trade winds increase.

The multiple controls on each potential trade wind proxy suggest that we must be

335 cautious in inferring past changes in trade winds and must evaluate the potential for other factors

to produce the observed signals. In this study, we focus on regions for which responses during

Heinrich stadials are recorded by multiple proxy types, as many of these proxies are reasonably

independent of each other (e.g. dust grain size vs. SSTs), and paired changes in records from the

same region are best explained by changes in winds. Where multiple proxy types are not

340 available, we evaluate the likelihood that the observed changes are the result of variations in

trade wind speed.

The trade wind proxies described above are interpreted qualitatively, as indicating either

increases or decreases in wind strength but not the magnitude of these changes. Sea surface and

subsurface temperature proxies can be compared directly between models and data to test

345 whether simulated wind changes are approximately similar to the changes reflected in proxy

records, as long as the seasonality and depth recorded by temperature proxies is understood (e.g.,

Tierney et al., 2015). Quantitative data-model comparisons are also possible for other proxies

through the use of forward models simulating proxy responses from model output ("proxy

system models"; Evans et al., 2013; Goose, 2016). Initial efforts have been made to model the

350 productivity and dust responses during Heinrich stadials and to compare simulated changes to

proxy data (Albani et al., 2016; Mariotti et al., 2012; Murphy et al., 2014). Further work building

on these studies may allow us to place quantitative bounds on past trade wind changes and to

better test data-model agreement.

355

4. Trade wind changes and ITCZ shifts in paleoclimate records

We now review evidence for changes in trade wind intensities during Heinrich stadials, which exhibit the largest perturbations to the balance of surface heating between the hemispheres (Figure 3A) and the clearest examples of shifts of the annual-mean ITCZ in the recent paleo-

360   record (Clement and Peterson, 2008; McGee et al., 2014; Schneider et al., 2014). We focus in particular on the most recent two stadials – Heinrich Stadial 1 (~18-15 ka) and the Younger Dryas (12.9-11.7 ka) – because of the increased data availability and data quality for these intervals, but we also examine previous Heinrich stadials when possible. We assess the robustness of proxy evidence for changes in the trade winds and then look for regional and

365   interhemispheric differences in trade wind responses to build a clearer picture of atmospheric circulation changes during these periods. Sediment core locations and a summary of observations from each core are included in Table 1.

4.1 Northern Hemisphere trade winds during Heinrich stadials

370   In the Northern Hemisphere, the clearest trade wind signals during Heinrich stadials are in the subtropical North Atlantic. Along the northwest African margin, a variety of marine sediment records document increases in windblown dust flux or dust abundance during Heinrich stadials (Figure 3D) (Adkins et al., 2006; Collins et al., 2013; McGee et al., 2013; Tjallingii et al., 2008). Records of biogenic sediment composition and flux from the NW African margin also

375   document increases in opal and organic carbon accumulation during Heinrich stadials (Figure 3E) (Bradtmiller et al., 2016; Romero et al., 2008). In addition, SST reconstructions from the region indicate SST minima during Heinrich stadials (Figure 3F) (Romero et al., 2008). Though each of these records in isolation could reflect other environmental factors, the dust, productivity

and SST records together paint a consistent picture of substantially intensified trade winds along

380   the NW African margin during Heinrich events (Bradtmiller et al., 2016; Romero et al., 2008), with the best data availability for HS1 and the YD. Based on the modern seasonality of coastal upwelling and dust transport in this region, it is most likely that these changes reflect increases in winter trade winds (Anderson et al., 2016; Bradtmiller et al., 2016; McGee et al., 2013). On the other side of the subtropical North Atlantic, high-resolution records from the Cariaco

385   Basin show evidence for SST cooling during the Younger Dryas and, to a lesser extent, during Heinrich Stadial 1 (Figure 3B) (Lea, 2003). The Younger Dryas and the end of Heinrich Stadial 1 are also marked by lighter sediment color, taken to represent increased surface productivity (Figure 3C) (Deplazes et al., 2013; Hughen et al., 1996), and increased abundance of upwelling-adapted species (*G. bulloides* and diatoms) (Dahl et al., 2004; Peterson et al., 1991). Longer

390   records suggest that similar changes in sediment color accompany stadials throughout the last glacial cycle (Deplazes et al., 2013). Together, these findings point to increased trade wind-driven upwelling in the western subtropical North Atlantic during Heinrich stadials, suggesting trade wind intensification across the breadth of the low-latitude North Atlantic. When compared with the modeling results shown in Fig. 2, we find best model–data agreement with the CM2Mc

395   model, where a clear pattern of intensified trade winds is simulated in the tropical North Atlantic.

In the Arabian Sea, southwesterly winds associated with the Indian summer monsoon drive upwelling and high productivity along the Oman and Somali margins during the summer months, and northeasterly winter winds reduce upwelling. Though this seasonal wind reversal characterizes the South Asian monsoon system, the winds project strongly onto the zonal mean

400   Hadley circulation and constitute a major portion of interhemispheric atmospheric heat transport associated with the annual mean, zonal mean tropical circulation (Heaviside and Czaja, 2013).
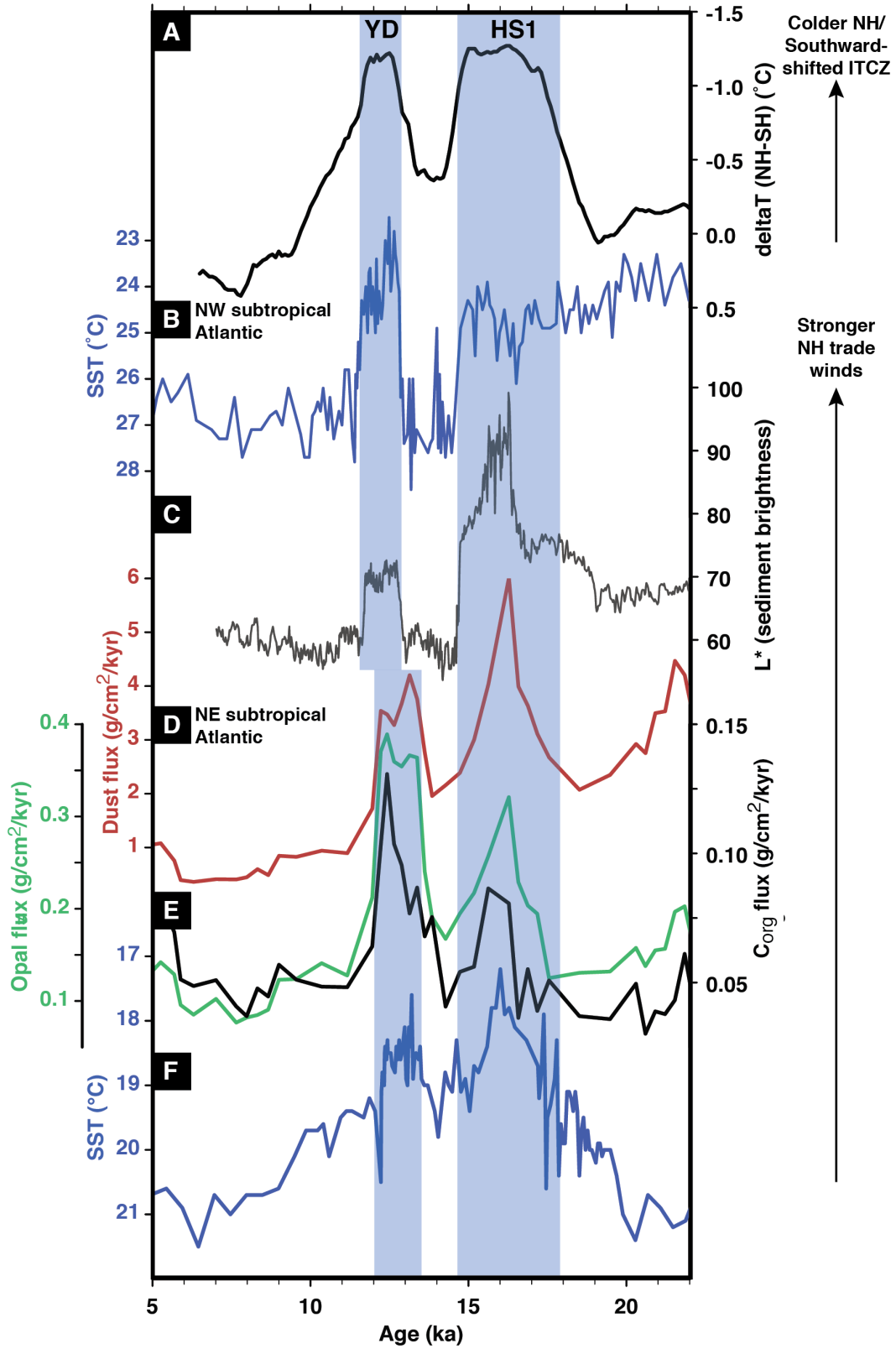
Figure 3. Examples of trade wind proxies from the North Atlantic showing evidence for NH
trade wind intensification in association with implied southward ITCZ shifts during Heinrich
Stadial 1 (HS1) and the Younger Dryas (YD). **A.** Reconstruction of hemispheric surface
temperature difference (Shakun et al., 2012); **B.** Mg/Ca-based SST reconstruction from Cariaco
Basin core PL07-39PC (Lea, 2003); **C.** Sediment color from Cariaco basin core MD03-2621,
with higher values interpreted as reflecting higher primary productivity (Deplazes et al., 2013);
D. Dust flux reconstruction from NW African margin core OCE437-7 GC68 (McGee et al.,
2013); **E.** Reconstructions of opal and organic carbon fluxes from NW African margin core
OCE437-7 GC68 (Bradtmiller et al., 2016); **F.** Alkenone-based SST data from NW African
margin core GeoB7926-2 (Romero et al., 2008). The offset in the age of the YD in the African
margin cores may reflect changes in surface water radiocarbon age in this region. Note flipped
vertical axis directions on temperature plots. Core locations listed in Table 1.

Because of the orientation of the coastline relative to the ocean and winds, strengthening of northeasterly trade winds in the Arabian Sea during stadials is expected to produce a reduction in upwelling, rather than an increase as observed along the northwest African margin. A variety of

420 proxy records of upwelling intensity and subsurface temperatures are consistent with a reduction in upwelling during Heinrich stadials throughout the last glacial period, as expected for a strengthening of northeasterly winds and/or a weakening of southwesterly summer monsoon winds. These records indicate reduced total organic carbon content in sediments (Schulz et al., 1998); nitrogen isotope data suggesting reduced water column denitrification, interpreted as

425 reflecting reduced oxygen demand from sinking organic matter (Altabet et al., 2002); and increased subsurface temperatures, consistent with reduced vertical mixing and heat loss to the atmosphere during winter (Huguet et al., 2006; Tierney et al., 2015). Dust fluxes in the Arabian Sea also increase substantially during Heinrich stadials (Pourmand et al., 2004), suggesting an increase in northerly winter winds transporting dust from the Arabian peninsula and South Asia.

430 Weakening of summer southwesterly winds and strengthening of winter northeasterly winds during stadials produce northeasterly wind anomalies in the annual mean that weaken both the lower branch of the zonally and annually averaged Hadley circulation and the wind-driven oceanic subtropical cell in the NH portion of the Indian Ocean (Section 5). Consistent with these reconstructed changes, the model simulations considered here show northerly and northeasterly

435 wind anomalies in the Arabian Sea in the annual mean (Figure 2a), as well as in both winter (DJF) and summer (JJA; not shown).

Reconstructing trade wind changes in the tropical and subtropical North Pacific poses a greater challenge. There are no high-resolution dust records reflecting short-range transport, as regional dust sources in the trade wind belt (e.g., the deserts of western Mexico) are weak.

440   Coastal upwelling records are complicated by the fact that most coastlines in the northeast

tropical Pacific trend southeast/northwest, orthogonal to canonical trade wind directions. As

detailed below, changes in the nutrient content and temperature of upwelled waters also obscure

interpretation of upwelling records.

      In Baja California, where wind-driven upwelling occurs throughout the year (Takesue et

445   al., 2004), marine sediments document minima in organic carbon accumulation and benthic

foraminifera abundance during most Heinrich stadials of the last 50 ka (Cartapanis et al., 2011;

Ortiz et al., 2004). Similarly, records from the Gulf of California indicate reduced opal

abundance and increasing SSTs during Heinrich stadials of the last 50 ka (Cheshire and Thurow,

2013; McClymont et al., 2012). These indications of reduced surface ocean productivity and

450   increasing SSTs may seem to indicate weakened trade winds during Heinrich stadials. However,

Ortiz et al. (2004) suggest that this pattern primarily reflects a shift to El Niño-like conditions in

the tropical Pacific during Heinrich stadials, which would lead to a deepened regional

thermocline/nutricline and thus a reduction in nutrient content and increase in temperature in

upwelled waters. Modern observations of upwelling and nutrients in southern Baja California

455   indicate that nutrient delivery to the surface can be reduced during and immediately following El

Niño events due to deepening of the regional nutricline even in the presence of strengthened

coast-parallel winds and upwelling intensity (Takesue et al., 2004). At present it is unclear

whether Heinrich stadials were characterized by El Niño- or La Niña-like mean states (e.g.,

Prange et al., 2010), or whether ENSO is an inappropriate analogue for regional ocean-

460   atmosphere changes during stadials (Leduc et al., 2009; McClymont et al., 2012). At the very

least, modern data suggest that upwelling records in the subtropical North Pacific may primarily

reflect changes in the equatorial Pacific thermocline rather than local trade wind strength.

Closer to the equator in the North Pacific, records of opal accumulation and diatom species assemblages at a coastal site off the Costa Rica margin in the Panama Basin indicate

465 lower nutrient supply and decreased opal flux during Heinrich stadials (Romero et al., 2011). These indicators of decreased upwelling are interpreted by the authors to represent increased northeasterly winds, as the site lies in the lee of the Central American highlands (Talamanca Cordillera) and experiences downwelling due to the wind stress curl driven by northeasterly wind jets traveling through topographic gaps (Romero et al., 2011). The speed of these wind jets

470 is correlated with regional trade wind strength (Chelton et al., 2000), supporting a connection between overall trade wind strength, wind jet strength, and downwelling intensification at this core site.

Just north of the equator in the eastern Pacific, Heinrich Stadial 1 and the Younger Dryas are marked by SST minima and maxima in organic carbon and opal accumulation rates (Kienast

475 et al., 2006). These changes are interpreted by the authors to reflect increased northeasterly trades during these periods, consistent with expectations. However, without more data it is not clear that we can rule out the possibility that these responses were caused by changes in the temperature or nutrient content of upwelled waters or changes in equator-crossing southeasterly trade winds.

480 Improved trade winds reconstructions in the Pacific would be valuable for clarifying equatorial Pacific ENSO dynamics and the Pacific ITCZ response during Heinrich stadials. Hosing simulations suggest that the trade wind-driven Pacific STC response to NH cooling plays a major role in increasing heat transport into the NH during stadials (Yang et al., 2017, 2013), and additional proxy data could assist in testing this simulated response. Proxy data are also of

485 particular value in this region because its modern climatology is poorly represented in models,

which tend to overestimate rain belt precipitation south of the equator (Oueslati and Bellon, 2015). As a result, model simulations of ITCZ responses to past climate changes in this region may not be accurate.

490 **4.2 Southern Hemisphere trade winds during Heinrich stadials**

The highest-quality trade wind-related records in the SH exist in the subtropical South Atlantic near the Benguela upwelling system. Records of windblown dust grain size indicate a rapid reduction in dust grain size off the coast of southwest Africa during HS1, reflecting reduced transport of coarse-grained dust from sources in the Kalahari Desert (Figure 4B) (Stuut 495 et al., 2002). Similar reductions appear to correspond to Heinrich stadials 2 through 5, though the age model of this core leaves uncertainty as to the precise timing of these events. As dust grain size is unlikely to respond so coherently to changes in aridity, and as there is no evidence for changes in distance to dust sources beyond the gradual impact of glacial-interglacial sea level changes, the authors interpret these changes as reflecting the strength of dust-generating trade 500 winds.

Nearby in the northern portion of the Benguela upwelling system, Little et al. (1997) find reductions in upwelling-sensitive coldwater species (left-coiling *N. pachyderma*) during Heinrich stadials of the last 50 ka, including a large reduction during HS4 and a rapid decline at the beginning of HS1 (Figure 4). The authors interpret this result as reflecting reduced trade wind 505 intensity during Heinrich stadials. Finally, alkenone-based SST records suggest pronounced warming in the Benguela system during HS1 (Kim et al., 2003, 2002). Taken together, these dust grain size, faunal abundance and SST data suggest reductions in trade wind strength in the southeast Atlantic during Heinrich stadials.
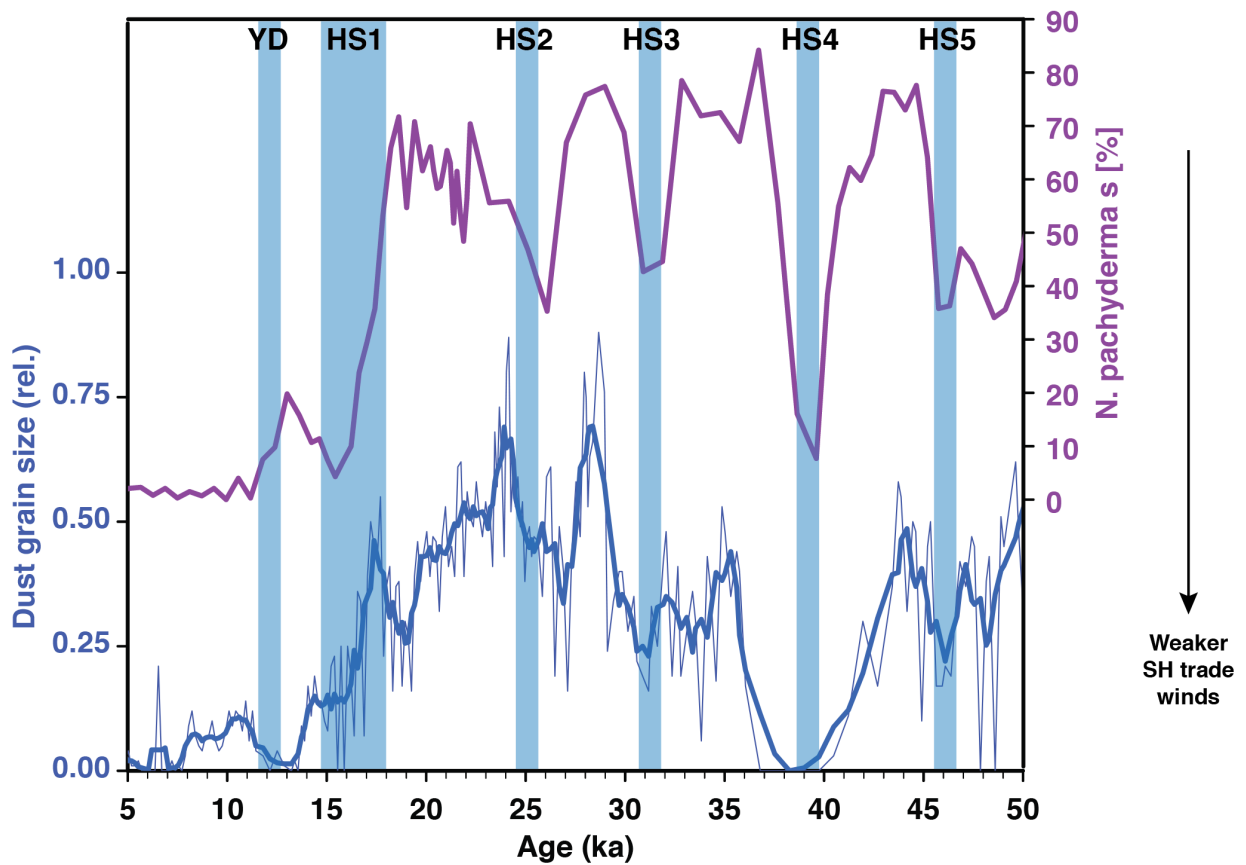
Figure 4. Trade wind proxies from the South Atlantic showing evidence for trade wind weakening in association with southward ITCZ shifts during Heinrich stadials of the last 50 ka. **A.** Abundance of *N. pachyderma* (left-coiling), an indicator of reduced SSTs and increased upwelling, in core GeoB1711-4 (Little et al., 1997). **B.** Dust grain size, expressed as the relative abundance of coarse-grained dust to total windblown dust, in core MD96-2094 (Stuut et al., 2002). Core locations listed in Table 1.

Fewer wind-related records are available in other regions of the SH subtropics. In marine sediments from the Peruvian margin, Saukel (2011) documents a rapid reduction in windblown

520   dust flux early in the deglaciation. This core site primarily receives windblown dust from the Atacama Desert (Saukel et al., 2011), a region that has been dry for at least the last 2 million years (Amundson et al., 2012); as a result, dust fluxes are unlikely to be modulated by aridity changes and are likely to directly reflect changes in surface wind strength, making this in excellent region for dust-based reconstructions of

525   winds. Similarly, a record of dust abundance from the eastern Indian Ocean off the coast of northwestern Australia suggests steep drops in dust abundance and grain size during the deglaciation (Stuut et al.,

2014). Unfortunately, neither of these records has the chronological control or temporal resolution necessary to pin down the timing of these deglacial declines in dust flux or to

530   document changes during previous Heinrich stadials, but the steep one-step drops are similar to the changes recorded in the southeast Atlantic during HS1.

These dust and upwelling records suggest reductions in trade wind intensity in the South Atlantic during Heinrich stadials. As shown in Figure 2, models suggest a clear pattern of weakened trade winds in all oceanic basins of the SH in association with a southward ITCZ shift,

535   but improved records from the South Pacific and South Indian Oceans are needed to test for similar responses in these regions. One puzzle is that SH records do not suggest coherent fluctuations in trade wind strength after HS1 during the Antarctic Cold Reversal/Bølling-Allerød interstadial and Younger Dryas stadial. In part, this may reflect the fact that some proxy systems used in these records (e.g. dust grain size, dust flux, *N. pachyderma s.* abundance) become less

540   sensitive in warmer climates that may have overall weaker trade winds and warmer ocean

temperatures. However, some records suggest cooling of Benguela region SSTs during the YD, a response opposite to that expected in response to a southward shift of the ITCZ at this time (Farmer et al., 2005; Kim et al., 2003, 2002). Further research is required to better document upwelling and dust changes in the SH during the latter half of the deglaciation.

545

5. Discussion: **Significance of trade wind changes during Heinrich stadials**

Taken together, these data point to systematic strengthening of NH trade winds and weakening of SH trade winds in the Atlantic basin during Heinrich stadials (Figure 5), with some indications of similar responses in the Pacific and Indian basins. This asymmetric response is

550   consistent with that predicted in association with a southward ITCZ shift, as the southerly location of the ITCZ is expected to lead to an intensification of the NH Hadley cell and associated trade winds and a weakening of the SH Hadley cell and trade winds (Section 2).

The finding of asymmetric trade wind responses during stadial events in proxy data is significant for several reasons. First, it reinforces reconstructions of southward shifts of the ITCZ

555   during Heinrich stadials based on precipitation proxies (Hodell et al., 2008; Peterson, 2000; Wang et al., 2004) and tropical SST gradients (McGee et al., 2014). This finding thus further strengthens the relationship between asymmetric high-latitude cooling, hemispheric energy budgets, ITCZ location and Hadley cell strengthening/weakening that is central to our understanding of ITCZ position and Hadley cell dynamics (Chiang and Friedman, 2012;

560   Donohoe et al., 2013; Kang et al., 2008; Marshall et al., 2014; Schneider et al., 2014). Asymmetric trade wind responses also suggest that WES feedbacks may have played a significant role in communicating high-latitude Northern Hemisphere cooling to the tropical North Atlantic (Chiang and Bitz, 2005). Enhanced North Atlantic boreal winter trade winds also
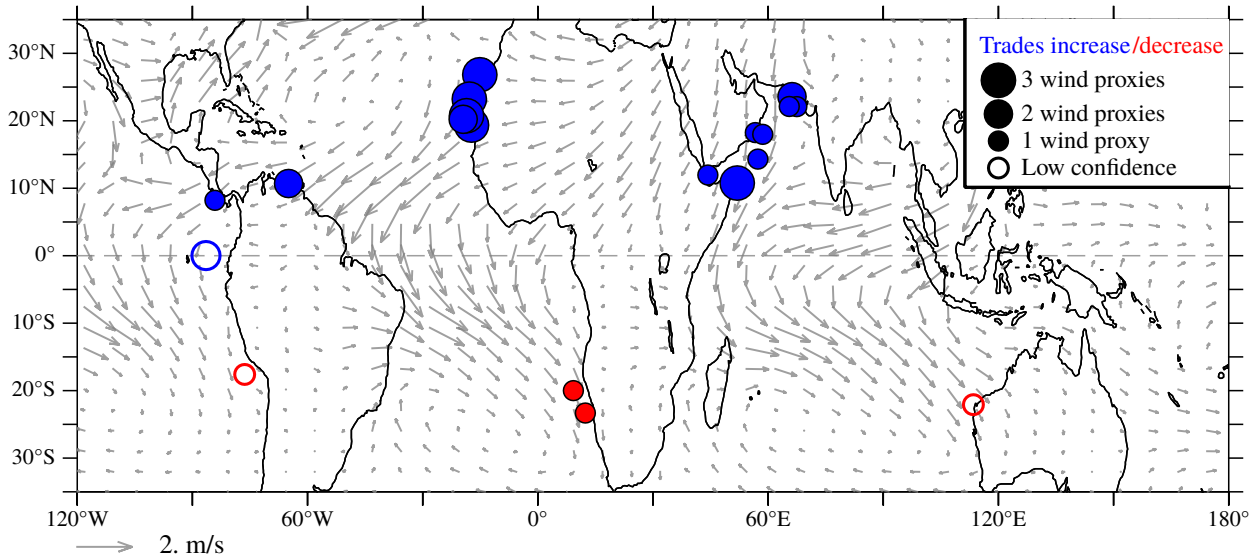
Figure 5. Map of proxy inferences of trade wind changes during Heinrich stadials on top of map of annually averaged near-surface wind anomalies (10 m) from the CM2Mc hosing experiment, from Figure 2A. Blue: implied increase in trade wind strength. Red: implied decrease in trade wind strength. Symbol size indicates the number of trade wind proxies (e.g., SSTs, productivity, dust flux) available at each site. Empty symbols indicate records with insufficient chronological control or temporal resolution or with questions as to their interpretation. Some symbols have been slightly displaced to make them visible on the map.

are likely to have played a role in advecting moisture into northern South America (Garcia and

Kayano, 2010; Vuille et al., 2012), leading to strengthening of the South American summer

575   monsoon during Heinrich stadials as observed in proxy data (Baker and Fritz, 2015; Placzek et

al., 2006; Stríkis et al., 2015; Wang et al., 2017, 2007). Such an increase is consistent with the

anomalous precipitation pattern that is simulated with the CM2Mc model, yet it clearly disagrees

with the one in the TraCE-21ka simulation during HS1 (Fig. 2A).

Hemispherically asymmetric trade wind changes are also likely to have altered the

580   strength of the ocean's overturning STCs, in which waters move from equatorial regions to the

subtropics at the surface, then sink and return to low latitudes at thermocline depths (~300-400

m) (Section 2.3). Though these cells are much shallower than the ocean's deep overturning

circulation, they transport a similar magnitude of heat due to the large difference in temperature

between the upper and lower limbs (Held, 2001; Klinger and Marotzke, 2000). In response to

585   strengthening of NH trade winds and weakening of SH trade winds, an anomalous shallow cross-

equatorial circulation develops that transports surface waters and heat from the SH into the NH

(Figure 6A). This increased northward heat transport in the shallow ocean offsets a significant

portion (~30-40%) of the ocean heat transport anomaly associated with reductions in AMOC in

GCM hosing simulations designed to resemble Heinrich stadials (Yang et al., 2017, 2013). In

590   idealized simulations by Green and Marshall (2017) in which hemispheric energy budgets are

perturbed, ITCZ shifts in fully coupled ocean-atmosphere simulations are much smaller than

shifts in uncoupled (slab ocean) experiments (Figure 6B). The authors attribute most of this

difference to the role of the oceans' subtropical cells in amplifying the heat transport into the

cooler hemisphere associated with an ITCZ shift (Green and Marshall, 2017).

595   The large changes in cross-equatorial atmospheric heat transport that accompany

relatively small (1-2 degrees latitude) changes in zonal mean ITCZ position make it unlikely that

the ITCZ has been far from the equator in the past unless heat transports associated with the

Hadley circulation were very different (Donohoe et al., 2013; McGee et al., 2014). The STC

response to ITCZ shifts further decreases the likelihood that the ITCZ was located far from the

600   equator in past climates, as it increases the interhemispheric energy transport anomalies

associated with ITCZ shifts. Windblown dust provenance data from the Pacific Ocean tracing the

latitudinal transition from sediment compositions similar to Asian dust (found north of the ITCZ

today) to compositions similar to volcanic inputs and/or American dust (found south of the ITCZ

today) have been interpreted as suggesting that the Pacific ITCZ was located at 30˚N at 40 Ma

605   and 12˚N as recently as 8 Ma (Hyeong et al., 2005; Lyle et al., 2002; Pettke, 2002). As the

position of the Pacific ITCZ strongly influences the zonal-mean, annual-mean ITCZ position,

these studies suggest either radically weaker heat transports associated with the Hadley cells and

STCs in these warmer climates, very strong heating differences between the hemispheres, or the

need for alternative interpretations of the dust provenance data. In particular, the northerly

610   position of the dust provenance transition in the mid-Cenozoic may reflect low Asian dust inputs

prior to the Pliocene (An et al., 2001; Zhang et al., 2016) rather than a dramatic change in ITCZ

location; strongly reduced Asian dust flux and relatively constant inputs of volcanic ash and dust
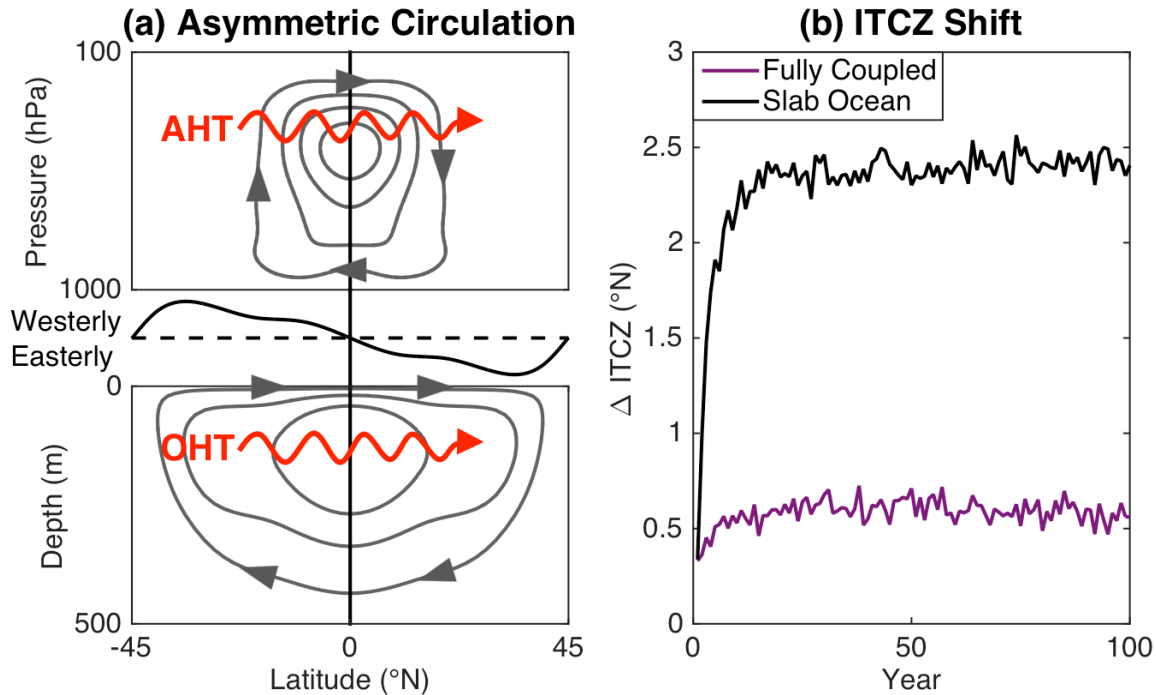
Figure 6. The tropical atmosphere and ocean response to NH cooling. **A.** Anomalies in zonal mean, annual mean atmospheric and shallow ocean circulation in response NH cooling. Top panel shows anomalies in Hadley circulation; middle panel shows changes in zonal component of near-surface winds, showing strengthening of easterly winds in the NH and weakening in the SH; bottom panel shows resulting shallow ocean circulation anomalies. The anomalous atmospheric and ocean circulations both act to transport heat into the NH (thick arrows). Contours indicate stream function anomalies. **B.** ITCZ shifts in response to cooling of one hemisphere in idealized climate model simulations. The black line shows a large ITCZ shift toward the warmer hemisphere in an uncoupled "slab" ocean simulation. The purple line shows a much smaller ITCZ shift in response to the same perturbation in a coupled simulation; the smaller response is primarily due to heat transport associated with the anomalous tropical ocean circulation shown in panel A. Note that the cooling perturbation and ITCZ responses in this simulation are not meant to resemble those during a Heinrich stadial, only to demonstrate the

role of the ocean in reducing the likelihood of extreme ITCZ shifts. Adapted from Green and

Marshall (2017).

630

from sources in the Americas would be expected to lead to a stronger volcanic/American dust signature in subtropical Pacific sediments regardless of ITCZ changes.

6. Conclusion and directions for future research

635   Trade wind-sensitive proxies from Atlantic Ocean sites suggest that trade winds intensified in the NH subtropics and weakened in the SH subtropics during millennial-scale NH cooling events. Wind proxies in the Arabian Sea and eastern equatorial Pacific also indicate intensification of NH trade winds during stadials. Angular momentum constraints and model results indicate that these asymmetric trade wind changes are the expected response to cooling of

640   the NH relative to the SH, as a southward ITCZ shift is accompanied by an intensification of the NH Hadley cell and associated trade winds, with an opposite response in the SH.

      The coherent response of trade wind proxies during stadials demonstrates the potential of trade wind-sensitive proxies to trace ITCZ shifts and Hadley cell changes. As shown in the maps of Figure 2, trade wind anomalies have strong spatial coherence, particularly over the subtropical

645   oceans, making wind reconstructions highly representative of regional circulation changes. Wind-based proxies may be particularly valuable in regions and time periods for which precipitation proxies are scarce or difficult to interpret, but even in well-studied intervals they offer valuable independent insights into the tropical atmosphere's response to past climate changes.

650   This work suggests several important avenues for future research building upon the use of trade wind proxies to track ITCZ and Hadley cell changes. The lack of high-resolution, precisely dated trade wind proxy records in the southeastern Indian and southeastern Pacific Ocean presently limits our ability to trace trade wind responses to stadial events outside of the

Atlantic basin, highlighting the need for additional records. Better documentation of trade wind changes in the Pacific basin is particularly important for shedding light on the magnitude of ITCZ shifts and STC changes during stadials. Trade wind proxies may also be useful in testing ITCZ shifts and Hadley cell dynamics in climates warmer than the present (e.g., the Pliocene or Cretaceous) (Hasegawa et al., 2012) or times in the Cenozoic when very large (10-25˚) shifts of the ITCZ have been suggested based on dust provenance data (Lyle et al., 2002; Pettke, 2002). Modeling of upwelling and dust responses to wind variations may help constrain the trade wind changes necessary to explain proxy data and offer opportunities for quantitative data-model comparisons (Albani et al., 2016; Miller and Tziperman, 2017; Murphy et al., 2014).

Beyond tracing ITCZ shifts and Hadley cell strength, hemispherically asymmetric trade wind anomalies reconstructed here are expected to drive similar changes in the wind-driven ocean subtropical cells. This shallow ocean response to an ITCZ shift transports heat into the cooler hemisphere with a magnitude comparable to the anomalous atmospheric heat transport associated with the ITCZ shift itself; this amplifies heat transport anomalies associated with changes in the mean ITCZ position, thereby damping ITCZ variations induced by interhemispheric heating anomalies (Green and Marshall, 2017; Yang et al., 2017, 2013) and reducing the likelihood of extreme ITCZ shifts in the past. Understanding trade wind changes is thus essential not only to better constraining ITCZ shifts in past climates, but also to understanding the ocean and atmosphere dynamical changes that will determine the future response of the tropical circulation and precipitation to anthropogenic radiative forcing.

Acknowledgements

References

680 Adkins, J., deMenocal, P., Eshel, G., 2006. The "African humid period" and the record of marine
    upwelling from excess 230Th in Ocean Drilling Program Hole 658C. Paleoceanography 21,
    1–14. doi:10.1029/2005PA001200

Albani, S., Mahowald, N.M., Murphy, L.N., Raiswell, R., Moore, J.K., Anderson, R.F., Mcgee,
    D., Bradtmiller, L.I., Delmonte, B., Hesse, P.P., Mayewski, P.A., 2016. Paleodust
685   variability since the Last Glacial Maximum and implications for iron inputs to the ocean.
    Geophys. Res. Lett. 3944–3954. doi:10.1002/2016GL067911

Alley, R.B., Meese, D.A., Shuman, C.A., Gow, A.J., Taylor, K.C., Grootes, P.M., White, J.W.C.,
    Ram, M., Waddington, E.D., Mayewski, P.A., Zielinski, G.A., 1993. Aburpt increase in
    Greenland snow accumulation at the end of the Younger Dryas event. Nature 362, 527–529.
690   doi:10.1038/362527a0

Altabet, M.A., Higginson, M.J., Murray, D.W., 2002. The effect of millennial-scale changes in
    Arabian Sea denitrification on atmospheric CO_2. Nature 415, 159–162.
    doi:10.1038/415159a

Amrhein, D.E., Gebbie, G., Marchal, O., Wunsch, C., 2015. Inferring surface water equilibrium
695   calcite delta O-18 during the last deglacial period from benthic foraminiferal records:
    Implications for ocean circulation. Paleoceanography 30, 1470–1489.
    doi:10.1002/2014PA002743

Amundson, R., Dietrich, W., Bellugi, D., Ewing, S., Nishiizumi, K., Chong, G., Owen, J., Finkel,
    R., Heimsath, A., Stewart, B., Caffee, M., 2012. Geomorphologic evidence for the late
700   Pliocene onset of hyperaridity in the Atacama Desert. Bull. Geol. Soc. Am. 124, 1048–
    1070. doi:10.1130/B30445.1

An, Z., Kutzbach, J.E., Prell, W.L., Porter, S.C., 2001. Evolution of Asian monsoons and phased
    uplift of the Himalaya-Tibetan plateau since Late Miocene times. Nature 411, 62–66.
    doi:10.1038/35075035

705 Anderson, R.F., Cheng, H., Edwards, R.L., Fleisher, M.Q., Hayes, C.T., Huang, K.-F., Kadko,
    D., Lam, P.J., Landing, W.M., Lao, Y., 2016. How well can we quantify dust deposition to
    the ocean? Phil. Trans. R. Soc. A 374, 20150285. doi:10.1098/rsta.2015.0285

Arbuszewski, J.A., deMenocal, P.B., Cléroux, C., Bradtmiller, L., Mix, A., 2013. Meridional
    shifts of the Atlantic intertropical convergence zone since the Last Glacial Maximum. Nat.
710   Geosci. 6, 959–962. doi:10.1038/ngeo1961

Baker, P.A., 2001. The History of South American Tropical Precipitation for the Past 25,000
    Years. Science 291, 640–643. doi:10.1126/science.291.5504.640

Baker, P.A., Fritz, S.C., 2015. Nature and causes of Quaternary climate variation of tropical

South America. Quat. Sci. Rev. 124, 31–47. doi:10.1016/j.quascirev.2015.06.011

715   Barbante, C., Barnola, J.-M., Becagli, S., Beer, J., Bigler, M., Boutron, C., Blunier, T., Castellano, E., Cattani, O., Chappellaz, J., Dahl-Jensen, D., Debret, M., Delmonte, B., Dick, D., Falourd, S., Faria, S., Federer, U., Fischer, H., Freitag, J., Frenzel, A., Fritzsche, D., Fundel, F., Gabrielli, P., Gaspari, V., Gersonde, R., Graf, W., Grigoriev, D., Hamann, I., Hansson, M., Hoffmann, G., Hutterli, M.A., Huybrechts, P., Isaksson, E., Johnsen, S.,

720   Jouzel, J., Kaczmarska, M., Karlin, T., Kaufmann, P., Kipfstuhl, S., Kohno, M., Lambert, F., Lambrecht, A., Lambrecht, A., Landais, A., Lawer, G., Leuenberger, M., Littot, G., Loulergue, L., Lüthi, D., Maggi, V., Marino, F., Masson-Delmotte, V., Meyer, H., Miller, H., Mulvaney, R., Narcisi, B., Oerlemans, J., Oerter, H., Parrenin, F., Petit, J.-R., Raisbeck, G., Raynaud, D., Röthlisberger, R., Ruth, U., Rybak, O., Severi, M., Schmitt, J., Schwander,

725   J., Siegenthaler, U., Siggaard-Andersen, M.-L., Spahni, R., Steffensen, J.P., Stenni, B., Stocker, T.F., Tison, J.-L., Traversi, R., Udisti, R., Valero-Delgado, F., van den Broeke, M.R., van de Wal, R.S.W., Wagenbach, D., Wegner, A., Weiler, K., Wilhelms, F., Winther, J.-G., Wolff, E., 2006. One-to-one coupling of glacial climate variability in Greenland and Antarctica. Nature 444, 195–198. doi:10.1038/nature05301

730   Barker, S., Diz, P., Vautravers, M.J., Pike, J., Knorr, G., Hall, I.R., Broecker, W.S., 2009. Interhemispheric Atlantic seesaw response during the last deglaciation. Nature 457, 1097–1102. doi:10.1038/nature07770

Blunier, T., Brook, E.J., 2001. Timing of millennial-scale climate change in Antarctica and Greenland during the last glacial period. Science 291, 109–112.

735   doi:10.1126/science.291.5501.109

Blunier, T., Chappellaz, J., Schwander, J., Dallenbach, A., Stauffer, B., Stocker, T.F., Raynaud, D., Jouzel, J., Clausen, H.B., Hammer, C.U., Johnsen, S.J., 1998. Asynchrony of Antarctic and Greenland climate change during the last glacial period. Nature 394, 739–743. doi:10.1038/29447

740   Bond, G., Broecker, W., Johnsen, S., McManus, J., Labeyrie, L., Jouzel, J., Bonani, G., 1993. Correlations between climate records from North Atlantic sediments and Greenland ice. Nature 365, 143–147.

Boyle, E.A., Keigwin, L., 1987. North Atlantic thermohaline circulation during the past 20,000 years linked to high-latitude surface temperature. Nature. doi:10.1038/330035a0

745   Bradtmiller, L.I., McGee, D., Awalt, M., Evers, J., Yerxa, H., Kinsley, C.W., DeMenocal, P.B., 2016. Changes in biological productivity along the northwest African margin over the past 20,000 years. Paleoceanography 31, 1–18. doi:10.1002/2015PA002862

Broccoli, A.J., Dahl, K.A., Stouffer, R.J., 2006. Response of the ITCZ to Northern Hemisphere cooling. Geophys. Res. Lett. 33, n/a-n/a. doi:10.1029/2005GL024546

750   Broecker, W.S., 1998. Paleocean circulation during the Last Deglaciation: A bipolar seesaw? Paleoceanography 13, 119. doi:10.1029/97PA03707

Broecker, W.S., Putnam, A.E., 2013. Hydrologic impacts of past shifts of Earth's thermal equator offer insight into those to be produced by fossil fuel CO2. Proc. Natl. Acad. Sci. 110, 16710–16715. doi:10.1073/pnas.1301855110

755   Brown, N., Galbraith, E.D., 2016. Hosed vs. unhosed: Interruptions of the Atlantic Meridional Overturning Circulation in a global coupled model, with and without freshwater forcing. Clim. Past 12, 1663–1679. doi:10.5194/cp-12-1663-2016

Buizert, C., Adrian, B., Ahn, J., Albert, M., Alley, R.B., Baggenstos, D., Bauska, T.K., Bay, R.C., Bencivengo, B.B., Bentley, C.R., Brook, E.J., Chellman, N.J., Clow, G.D., Cole-Dai,

760   J., Conway, H., Cravens, E., Cuffey, K.M., Dunbar, N.W., Edwards, J.S., Fegyveresi, J.M., Ferris, D.G., Fitzpatrick, J.J., Fudge, T.J., Gibson, C.J., Gkinis, V., Goetz, J.J., Gregory, S., Hargreaves, G.M., Iverson, N., Johnson, J.A., Jones, T.R., Kalk, M.L., Kippenhan, M.J., Koffman, B.G., Kreutz, K., Kuhl, T.W., Lebar, D.A., Lee, J.E., Marcott, S.A., Markle, B.R., Maselli, O.J., McConnell, J.R., McGwire, K.C., Mitchell, L.E., Mortensen, N.B., Neff,
765   P.D., Nishiizumi, K., Nunn, R.M., Orsi, A.J., Pasteris, D.R., Pedro, J.B., Pettit, E.C., Buford Price, P., Priscu, J.C., Rhodes, R.H., Rosen, J.L., Schauer, A.J., Schoenemann, S.W., Sendelbach, P.J., Severinghaus, J.P., Shturmakov, A.J., Sigl, M., Slawny, K.R., Souney, J.M., Sowers, T.A., Spencer, M.K., Steig, E.J., Taylor, K.C., Twickler, M.S., Vaughn, B.H., Voigt, D.E., Waddington, E.D., Welten, K.C., Wendricks, A.W., White, J.W.C., Winstrup,
770   M., Wong, G.J., Woodruff, T.E., 2015. Precise interpolar phasing of abrupt climate change during the last ice age. Nature 520, 661–665. doi:10.1038/nature14401

Cartapanis, O., Tachikawa, K., Bard, E., 2011. Northeastern Pacific oxygen minimum zone variability over the past 70 kyr: Impact of biological production and oceanic ventilation. Paleoceanography 26, 1–17. doi:10.1029/2011PA002126

775 Chelton, D., Freilich, M., Esbensen, S., 2000. Satellite observations of the wind jets off the Pacific coast of Central America. Part I: Case studies and statistical characteristics. Mon. Wea. Rev. 128, 1993–2018. doi:10.1175/1520-0493(2000)128<1993:SOOTWJ>2.0.CO;2

Cheshire, H., Thurow, J., 2013. High-resolution migration history of the Subtropical High/Trade Wind system of the northeastern Pacific during the last 55 years: Implications for glacial
780   atmospheric reorganization. Paleoceanography 28, 319–333. doi:10.1002/palo.20031

Chiang, J.C.H., 2003. Sensitivity of the Atlantic Intertropical Convergence Zone to Last Glacial Maximum boundary conditions. Paleoceanography 18, 1–18. doi:10.1029/2003PA000916

Chiang, J.C.H., Bitz, C.M., 2005. Influence of high latitude ice cover on the marine Intertropical Convergence Zone. Clim. Dyn. 25, 477–496. doi:10.1007/s00382-005-0040-5

785 Chiang, J.C.H., Friedman, A.R., 2012. Extratropical Cooling, Interhemispheric Thermal Gradients, and Tropical Climate Change. Annu. Rev. Earth Planet. Sci. 40, 383–412. doi:10.1146/annurev-earth-042711-105545

Clement, A.C., Peterson, L.C., 2008. Mechanisms of Abrupt Climate Change of the Last Glacial Period. North 46, 1–39. doi:10.1029/2006RG000204

790 Collins, J.A., Govin, A., Mulitza, S., Heslop, D., Zabel, M., Hartmann, J., Röhl, U., Wefer, G., 2013. Abrupt shifts of the Sahara-Sahel boundary during Heinrich stadials. Clim. Past 9, 1181–1191. doi:10.5194/cp-9-1181-2013

Dahl, K.A., Repeta, D.J., Goericke, R., 2004. Reconstructing the phytoplankton community of the Cariaco Basin during the Younger Dryas cold event using chlorin steryl esters.
795   Paleoceanography 19, 1–13. doi:10.1029/2003PA000907

Dahl, K., Broccoli, A., Stouffer, R., 2005. Assessing the role of North Atlantic freshwater forcing in millennial scale climate variability: a tropical Atlantic perspective. Clim. Dyn. 24, 325–346. doi:10.1007/s00382-004-0499-5

Dail, H., Wunsch, C., 2014. Dynamical Reconstruction of Upper-Ocean Conditions in the Last
800   Glacial Maximum Atlantic. J. Clim. 27, 807–823. doi:10.1175/JCLI-D-13-00211.1

Dansgaard, W., Clausen, H.B., Gundestrup, N., Hammer, C.U., Johnsen, S.F., Kristinsdottir, P.M., Reeh, N., 1982. A new Greenland deep ice core. Science 218, 1273–1277. doi:10.1126/science.218.4579.1273

Deplazes, G., Lückge, A., Peterson, L.C., Timmermann, A., Hamann, Y., Hughen, K.A., Röhl,
805   U., Laj, C., Cane, M.A., Sigman, D.M., Haug, G.H., 2013. Links between tropical rainfall

and North Atlantic climate during the last glacial period. Nat. Geosci. 6, 1–5. doi:10.1038/ngeo1712

Donohoe, A., Marshall, J., Ferreira, D., Mcgee, D., 2013. The Relationship between ITCZ Location and Cross-Equatorial Atmospheric Heat Transport: From the Seasonal Cycle to the Last Glacial Maximum. J. Clim. 26, 3597–3618. doi:10.1175/JCLI-D-12-00467.1

Evans, M.N., Tolwinski-Ward, S.E., Thompson, D.M., Anchukaitis, K.J., 2013. Applications of proxy system modeling in high resolution paleoclimatology. Quat. Sci. Rev. 76, 16–28. doi:10.1016/j.quascirev.2013.05.024

Farmer, E.C., deMenocal, P.B., Marchitto, T.M., 2005. Holocene and deglacial ocean temperature variability in the Benguela upwelling region: Implications for low-latitude atmospheric circulation. Paleoceanography 20, 1–16. doi:10.1029/2004PA001049

Galbraith, E.D., Merlis, T.M., Palter, J.B., 2016. Destabilization of glacial climate by the radiative impact of Atlantic Meridional Overturning Circulation disruptions. Geophys. Res. Lett. 43, 8214–8221. doi:10.1002/2016GL069846

Garcia, S.R., Kayano, M.T., 2010. Some evidence on the relationship between the South American monsoon and the Atlantic ITCZ. Theor. Appl. Climatol. 99, 29–38. doi:10.1007/s00704-009-0107-z

Gillette, D.A., 1974. On the production of soil wind erosion aerosols having the potential for long range transport. J. Rech. Atmos. 8, 735–744.

Goose, H., 2016. An additional step toward comprehensive paleoclimate reanalyses. J. Adv. Model. Earth Syst. 8, 1501–1503. doi:doi:10.1002/ 2016MS000739

Green, B., Marshall, J., 2017. Coupling of Trade Winds with Ocean Circulation Damps ITCZ Shifts. J. Clim. JCLI-D-16-0818.1. doi:10.1175/JCLI-D-16-0818.1

Grini, A., Zender, C.S., 2004. Roles of saltation, sandblasting, and wind speed variability on mineral dust aerosol size distribution during the Puerto Rican Dust Experiment (PRIDE). J. Geophys. Res. 109, 1–12. doi:10.1029/2003JD004233

Hasegawa, H., Tada, R., Jiang, X., Suganuma, Y., Imsamut, S., Charusiri, P., Ichinnorov, N., Khand, Y., 2012. Drastic shrinking of the Hadley circulation during the mid-Cretaceous Supergreenhouse. Clim. Past 8, 1323–1337. doi:10.5194/cp-8-1323-2012

Heaviside, C., Czaja, a., 2013. Deconstructing the Hadley cell heat transport. Q. J. R. Meteorol. Soc. 139, 2181–2189. doi:10.1002/qj.2085

Held, I.M., 2001. The Partitioning of the Poleward Energy Transport between the Tropical Ocean and Atmosphere. J. Atmos. Sci. 58, 943–948. doi:10.1175/1520-0469(2001)058<0943:TPOTPE>2.0.CO;2

Hemming, S.R., 2004. Heinrich events: Massive late Pleistocene ditritus layers of the North Atlanitc and their global cliamate imprint. Rev. Geophys. 42. doi:10.1029/2003RG000128.1.INTRODUCTION

Henry, L.G., Mcmanus, J.F., Curry, W.B., Roberts, N.L., Piotrowski, A.M., Keigwin, L.D., 2016. North Atlantic ocean circulation and abrupt climate change during the last glaciation. Science 5529, 470–474. doi:10.1126/science.aaf5529

Hodell, D.A., Anselmetti, F.S., Ariztegui, D., Brenner, M., Curtis, J.H., Gilli, A., Grzesik, D.A., Guilderson, T.J., Müller, A.D., Bush, M.B., 2008. An 85-ka record of climate change in lowland Central America. Quat. Sci. Rev. 27, 1152–1165. doi:10.1016/j.quascirev.2008.02.008

Hughen, K.A., Overpeck, J.T., Peterson, L.C., Trumbore, S., 1996. Rapid climate changes in the tropical Atlantic region during the last deglaciation. Nature. doi:10.1038/380051a0

Huguet, C., Kim, J.H., Damsté, J.S.S., Schouten, S., 2006. Reconstruction of sea surface temperature variations in the Arabian Sea over the last 23 kyr using organic proxies (TEX86 and U 37K′). Paleoceanography 21, 1–13. doi:10.1029/2005PA001215

855 Hyeong, K., Park, S.H., Yoo, C.M., Kim, K.H., 2005. Mineralogical and geochemical compositions of the eolian dust from the northeast equatorial Pacific and their implications on paleolocation of the Intertropical Convergence Zone. Paleoceanography 20, 1–11. doi:10.1029/2004PA001053

Kang, S.M., Held, I.M., Frierson, D.M.W., Zhao, M., 2008. The response of the ITCZ to
860 extratropical thermal forcing: Idealized slab-ocean experiments with a GCM. J. Clim. 21, 3521–3532. doi:10.1175/2007JCLI2146.1

Kienast, M., Kienast, S.S., Calvert, S.E., Eglinton, T.I., Mollenhauer, G., François, R., Mix, A.C., 2006. Eastern Pacific cooling and Atlantic overturning circulation during the last deglaciation. Nature 444, 512–512. doi:10.1038/nature05377

865 Kim, J.H., Schneider, R.R., Mulitza, S., Müller, P.J., 2003. Reconstruction of SE trade-wind intensity based on sea-surface temperature gradients in the Southeast Atlantic over the last 25 kyr. Geophys. Res. Lett. 30, 3–6. doi:10.1029/2003GL017557

Kim, J.H., Schneider, R.R., Müller, P.J., Wefer, G., 2002. Interhemispheric comparison of deglacial sea-surface temperature patterns in Atlantic eastern boundary currents. Earth
870 Planet. Sci. Lett. 194, 383–393. doi:10.1016/S0012-821X(01)00545-3

Klinger, B.A., Marotzke, J., 2000. Meridional heat transport by the subtropical cell. J. Phys. Oceanogr. 30, 696–705. doi:10.1175/1520-0485(2000)030<0696:MHTBTS>2.0.CO;2

Lea, D.W., 2003. Synchroneity of Tropical and High-Latitude Atlantic Temperatures over the Last Glacial Termination. Science 301, 1361–1364. doi:10.1126/science.1088470

875 Leduc, G., Vidal, L., Tachikawa, K., Bard, E., 2009. ITCZ rather than ENSO signature for abrupt climate changes across the tropical Pacific? Quat. Res. 72, 123–131. doi:10.1016/j.yqres.2009.03.006

Li, C., Battisti, D.S., Schrag, D.P., Tziperman, E., 2005. Abrupt climate shifts in Greenland due to displacements of the sea ice edge 32, 2–5. doi:10.1029/2005GL023492

880 Little, M.G., Schneider, R.R., Kroon, D., Price, B., Summerhayes, C.P., Segl, M., 1997. Trade wind forcing of upwelling, seasonally, and Heinrich events as a response to sub-Milankovitch climate variability. Paleoceanography 12, 568–576. doi:10.1029/97PA00823

Liu, Z., Otto-Bliesner, B.L., He, F., Brady, E.C., Tomas, R., Clark, P.U., Carlson, A.E., Lynch-Stieglitz, J., Curry, W., Brook, E., Erickson, D., Jacob, R., Kutzbach, J., Cheng, J., 2009.
885 Transient Simulation of Last Deglaciation with a New Mechanism for Bolling-Allerod Warming. Science 325, 310–314. doi:10.1126/science.1171041

Lyle, M., Wilson, P.A., Janacek, T.R., 2002. Leg 199 Summary, in: Proceedings of the Ocean Drilling Program Initial Reports. pp. 1–87.

Mariotti, V., Bopp, L., Tagliabue, A., Kageyama, M., Swingedouw, D., 2012. Marine
890 productivity response to Heinrich events: A model-data comparison. Clim. Past 8, 1581–1598. doi:10.5194/cp-8-1581-2012

Marshall, J., Donohoe, A., Ferreira, D., McGee, D., 2014. The ocean's role in setting the mean position of the Inter-Tropical Convergence Zone. Clim. Dyn. 42, 1967–1979. doi:10.1007/s00382-013-1767-z

895 McClymont, E.L., Ganeshram, R.S., Pichevin, L.E., Talbot, H.M., Van Dongen, B.E., Thunell, R.C., Haywood, A.M., Singarayer, J.S., Valdes, P.J., 2012. Sea-surface temperature records of Termination 1 in the Gulf of California: Challenges for seasonal and interannual

analogues of tropical Pacific climate change. Paleoceanography 27, 1–15. doi:10.1029/2011PA002226

900   McCreary, Jr., J.P., Lu, P., 1994. Interaction between the Subtropical and Equatorial ocean circulations: The subtropical cell. J. Phys. Oceanogr. 24, 466–496.

McGee, D., Broecker, W.S., Winckler, G., 2010. Gustiness: The driver of glacial dustiness? Quat. Sci. Rev. 29, 2340–2350. doi:10.1016/j.quascirev.2010.06.009

McGee, D., deMenocal, P.B., Winckler, G., Stuut, J.B.W., Bradtmiller, L.I., 2013. The
905   magnitude, timing and abruptness of changes in North African dust deposition over the last 20,000 yr. Earth Planet. Sci. Lett. 371–372, 163–176. doi:10.1016/j.epsl.2013.03.054

McGee, D., Donohoe, A., Marshall, J., Ferreira, D., 2014. Changes in ITCZ location and cross-equatorial heat transport at the Last Glacial Maximum, Heinrich Stadial 1, and the mid-Holocene. Earth Planet. Sci. Lett. 390, 69–79. doi:10.1016/j.epsl.2013.12.043

910   Miller, M.D., Tziperman, E., 2017. The effect of changes in surface winds and ocean stratification on coastal upwelling and sea surface temperatures in the Pliocene. Paleoceanography. doi:10.1002/2016PA002996

Murphy, L.N., Clement, A.C., Albani, S., Mahowald, N.M., Swart, P., Arienzo, M.M., 2014. Simulated changes in atmospheric dust in response to a Heinrich stadial. Paleoceanography
915   29, 30–43. doi:10.1002/2013PA002550

Neelin, J.D., Held, I.M., 1987. Modeling tropical convergence based on the moist static energy budget. Mon. Weather Rev. 115, 3–12.

Ortiz, J.D., O'Connell, S.B., DelViscio, J., Dean, W., Carriquiry, J.D., Marchitto, T., Zheng, Y., van Geen, A., 2004. Enhanced marine productivity off western North America during warm
920   climate intervals of the past 52 k.y. Geology 32, 521–524. doi:10.1130/G20234.1

Oueslati, B., Bellon, G., 2015. The double ITCZ bias in CMIP5 models: interaction between SST, large-scale circulation and precipitation. Clim. Dyn. 44, 585–607. doi:10.1007/s00382-015-2468-6

Peterson, L.C., 2000. Rapid Changes in the Hydrologic Cycle of the Tropical Atlantic During the
925   Last Glacial. Science 290, 1947–1951. doi:10.1126/science.290.5498.1947

Peterson, L.C., Overpeck, J.T., Kipp, N.G., Imbrie, J., 1991. A high-resolution Late Quaternary upwelling record from the anoxic Cariaco Basin, Venezuela. Paleoceanography 6, 99–119.

Pettke, T., 2002. Cenozoic evolution of Asian climate and sources of Pacific seawater Pb and Nd derived from eolian dust of sediment core LL44-GPC3. Paleoceanography 17, 1–13.
930   doi:10.1029/2001PA000673

Placzek, C., Quade, J., Patchett, P.J., 2006. Geochronology and stratigraphy of late Pleistocene lake cycles on the southern Bolivian Altiplano: Implications for causes of tropical climate change. Bull. Geol. Soc. Am. 118, 515–532. doi:10.1130/B25770.1

Pourmand, A., Marcantonio, F., Schulz, H., 2004. Variations in productivity and eolian fluxes in
935   the northeastern Arabian Sea during the past 110 ka. Earth Planet. Sci. Lett. 221, 39–54. doi:10.1016/S0012-821X(04)00109-8

Prange, M., Steph, S., Schulz, M., Keigwin, L.D., 2010. Inferring moisture transport across Central America: Can modern analogs of climate variability help reconcile paleosalinity records? Quat. Sci. Rev. 29, 1317–1321. doi:10.1016/j.quascirev.2010.02.029

940   Rea, D.K., 1994. The paleoclimatic record provided by eolian deposition in the deep sea: The geologic history of wind. Rev. Geophys. 32, 159–195.

Romero, O.E., Kim, J.H., Donner, B., 2008. Submillennial-to-millennial variability of diatom production off Mauritania, NW Africa, during the last glacial cycle. Paleoceanography 23,

PA3218. doi:10.1029/2008PA001601

945   Romero, O.E., Leduc, G., Vidal, L., Fischer, G., 2011. Millennial variability and long-term changes of the diatom production in the eastern equatorial Pacific during the last glacial cycle. Paleoceanography 26, 1–11. doi:10.1029/2010PA002099

Roskin, J., Tsoar, H., Porat, N., Blumberg, D.G., 2011. Palaeoclimate interpretations of Late Pleistocene vegetated linear dune mobilization episodes: Evidence from the northwestern

950   Negev dunefield, Israel. Quat. Sci. Rev. 30, 3364–3380. doi:10.1016/j.quascirev.2011.08.014

Sachs, J.P., Sachse, D., Smittenberg, R.H., Zhang, Z., Battisti, D.S., Golubic, S., 2009. Southward movement of the Pacific intertropical convergence zone AD 1400–1850. Nat. Geosci. 2, 519–525. doi:10.1038/ngeo554

955   Sarnthein, M., Tetzlaff, G., Koopmann, B., Wolter, K., Pflaumann, U., 1981. Glacial and interglacial wind regimes over the eastern subtropical Atlantic and North-West Africa. Nature 293, 193–196. doi:10.1038/293193a0

Saukel, C., 2011. Tropical Southeast Pacific continent-ocean-atmosphere linkages since the Pliocene inferred from eolian dust. University of Bremen.

960   Saukel, C., Lamy, F., Stuut, J.B.W., Tiedemann, R., Vogt, C., 2011. Distribution and provenance of wind-blown SE Pacific surface sediments. Mar. Geol. 280, 130–142. doi:10.1016/j.margeo.2010.12.006

Schneider, T., Bischoff, T., Haug, G.H., 2014. Migrations and dynamics of the intertropical convergence zone. Nature 513, 45–53. doi:10.1038/nature13636

965   Schulz, H., van Rad, U., Erlenkeuser, H., 1998. Correlation between Arabian Sea and Greenland climate oscillations of the past 110,000 years. Nature 393, 54–57. doi:10.1038/31750

Shakun, J.D., Clark, P.U., He, F., Marcott, S. a., Mix, A.C., Liu, Z., Otto-Bliesner, B., Schmittner, A., Bard, E., 2012. Global warming preceded by increasing carbon dioxide concentrations during the last deglaciation. Nature 484, 49–54. doi:10.1038/nature10915

970   Stríkis, N.M., Chiessi, C.M., Cruz, F.W., Vuille, M., Cheng, H., de Souza Barreto, E.A., Mollenhauer, G., Kasten, S., Karmann, I., Edwards, R.L., Bernal, J.P., Sales, H. dos R., 2015. Timing and structure of Mega-SACZ events during Heinrich Stadial 1. Geophys. Res. Lett. 42, 5477–5484. doi:10.1002/2015GL064048

Stuut, J.B.W., Prins, M.A., Schneider, R.R., Weltje, G.J., Fred Jansen, J.H., Postma, G., 2002. A

975   300-kyr record of aridity and wind strength in southwestern Africa: Inferences from grain-size distributions of sediments on Walvis Ridge, SE Atlantic. Mar. Geol. 180, 221–233. doi:10.1016/S0025-3227(01)00215-8

Stuut, J.B.W., Temmesfeld, F., De Deckker, P., 2014. A 550ka record of aeolian activity near north west cape, australia: Inferences from grain-size distributions and bulk chemistry of SE

980   indian ocean deep-sea sediments. Quat. Sci. Rev. 83, 83–94. doi:10.1016/j.quascirev.2013.11.003

Takesue, R.K., van Geen, A., Carriquiry, J.D., Ortiz, E., Godinez-Orta, L., Granados, I., Saldivar, M., Ortlieb, L., Escribano, R., Guzman, N., Castilla, J.C., Varas, M., Salamanca, M., Figueroa, C., 2004. Influence of coastal upwelling and El Nino-Southern Oscillation on

985   nearshore water along Baja California and Chile: Shore-based monitoring during 1997-2000. J. Geophys. Res. 109. doi:10.1029/2003JC001856

Taylor, K.C., Lamorey, G.W., Doyle, G.A., Alley, R.B., Grootes, P.M., Mayewski, P. a., White, J.W.C., Barlow, L.K., 1993. The "flickering switch" of late Pleistocene climate change. Nature 361, 432–436. doi:10.1038/361432a0

990 Tierney, J.E., Pausata, F.S.R., deMenocal, P., 2015. Deglacial Indian monsoon failure and North Atlantic stadials linked by Indian Ocean surface cooling. Nat. Geosci. 9, 46–50. doi:10.1038/ngeo2603

Timmermann, A., Krebs, U., Justino, F., Goosse, H., Ivanochko, T., 2005. Mechanisms for millennial-scale global synchronization during the last glacial period. Paleoceanography 20.
995 doi:10.1029/2004PA001090

Tjallingii, R., Claussen, M., Stuut, J.-B.W., Fohlmeister, J., Jahn, A., Bickert, T., Lamy, F., Röhl, U., 2008. Coherent high- and low-latitude control of the northwest African hydrological balance. Nat. Geosci. 1, 670–675. doi:10.1038/ngeo289

Trenberth, K.E., Caron, J.M., 2001. Estimates of Meridional Atmosphere and Ocean Heat
1000 Transports. J. Clim. 14, 3433–3443. doi:10.1175/1520-0442(2001)014<3433:EOMAAO>2.0.CO;2

Tsoar, H., 2005. Sand dunes mobility and stability in relation to climate. Phys. A Stat. Mech. its Appl. 357, 50–56. doi:10.1016/j.physa.2005.05.067

Vellinga, M., Wood, R.A., 2002. Global climatic impacts of a collapse of the Atlantic
1005 thermohaline circulation. Clim. Change 54, 251–267. doi:10.1023/A:1016168827653

Vuille, M., Burns, S.J., Taylor, B.L., Cruz, F.W., Bird, B.W., Abbott, M.B., Kanner, L.C., Cheng, H., Novello, V.F., 2012. A review of the South American monsoon history as recorded in stable isotopic proxies over the past two millennia. Clim. Past 8, 1309–1321. doi:10.5194/cp-8-1309-2012

1010 Wang, W., Evan, A., Flamant, C., Lavaysse, C., 2015. On the Decadal Scale Correlation between African Dust and Sahel Rainfall: the Role of Saharan Heat Low-Forced Winds. Sci. Adv. 1, e1500646.

Wang, X., Auler, A.S., Edwards, R.L., Cheng, H., Cristalli, P.S., Smart, P.L., Richards, D.A., Shen, C.-C., 2004. Wet periods in northeastern Brazil over the past 210 kyr linked to distant
1015 climate anomalies. Nature 432, 740–743. doi:10.1038/nature03067

Wang, X., Auler, A.S., Edwards, R.L., Cheng, H., Ito, E., Wang, Y., Kong, X., Solheid, M., 2007. Millennial-scale precipitation changes in southern Brazil over the past 90,000 years. Geophys. Res. Lett. 34, n/a-n/a. doi:10.1029/2007GL031149

Wang, X., Edwards, R.L., Auler, A.S., Cheng, H., Kong, X., Wang, Y., Cruz, F.W., Dorale, J.A.,
1020 Chiang, H.-W., 2017. Hydroclimate changes across the Amazon lowlands over the past 45,000 years. Nature 541, 204–207. doi:10.1038/nature20787

Wang, Y.J., 2001. A High-Resolution Absolute-Dated Late Pleistocene Monsoon Record from Hulu Cave, China. Science 294, 2345–2348. doi:10.1126/science.1064618

Yang, H., Wang, Y., Liu, Z., 2013. A modelling study of the Bjerknes compensation in the
1025 meridional heat transport in a freshening ocean. Tellus A 65, 18480. doi:10.3402/tellusa.v65i0.18480

Yang, H., Wen, Q., Yao, J., Wang, Y., 2017. Bjerknes Compensation in Meridional Heat Transport under Freshwater Forcing and the Role of Climate Feedback. J. Clim. 30, 5167–5185. doi:10.1175/JCLI-D-16-0824.1

1030 Zhang, R., Delworth, T.L., 2005. Simulated tropical response to a substantial weakening of the Atlantic thermohaline circulation. J. Clim. 18, 1853–1860. doi:10.1175/JCLI3460.1

Zhang, W., Chen, J., Ji, J., Li, G., 2016. Evolving flux of Asian dust in the North Pacific Ocean since the late Oligocene. Aeolian Res. 23, 1–11. doi:10.1016/j.aeolia.2016.09.004

Table 1. Core sites discussed in text.

Region	Core	Lat. (˚N)	Long. (˚E)	# wind proxies	Stadial trade wind change (+/-)	Confidence (1=high; 0=low)	Type(s) of proxies	References
S Atlantic	MD96-2094	-20.00	9.26	1	-	1	Dust grain size	Stuut et al., 2002
	GeoB1711-4	-23.32	12.38	1	-	1	Upwelling-associated foram species	Little et al., 1997
S Indian	MD00-2361	-22.08	113.48	1	-	0	Dust abundance	Stuut et al., 2015
S Pacific	ODP1237	-17.60	-76.38	1	-	0	Dust flux	Saukel, 2011
NE Atlantic	OCE437-7 GC68	19.36	-17.28	3	+	1	Dust, opal, organic C fluxes	McGee et al., 2013; Bradtmiller et al., 2016
	OCE437-7 GC49	23.21	-17.85	3	+	1	Dust, opal, organic C fluxes	McGee et al., 2013; Bradtmiller et al., 2016
	OCE437-7 GC37	26.82	-15.12	3	+	1	Dust, opal, organic C fluxes	McGee et al., 2013; Bradtmiller et al., 2016
	ODP 658	20.75	-18.58	3	+	1	Dust flux, opal flux, SST	Adkins et al., 2006; Zhao et al., 1995
	GeoB7926-2	20.22	-18.45	2	+	1	Opal/diatom abundance, SST	Romero et al., 2008
NW Atlantic	PL07-39PC/ MD03-2621	10.70	-64.94	2	+	1	SST, sediment color, upwelling species abundance	Lea et al., 2003, Deplazes et al., 2013
NE Pacific	ME0005A-24JC	0.02	-86.46	2	+	0	SST, organic C flux	Kienast et al., 2006
	MD02-2529	8.21	-84.12	1	+	1	Opal/diatom abundance	Romero et al., 2011
Arabian Sea	SO90-111KL	23.10	66.48	1	+	1	Organic C abundance	Schulz et al., 1998
	SO90-136KL	23.12	66.50	1	+	1	Organic C abundance	Schulz et al., 1998
	RC27-14	18.25	57.66	1	+	1	N isotopes	Altabet et al., 2002
	RC27-23	17.99	57.59	1	+	1	N isotopes	Altabet et al., 2002
	NIOP905	10.77	51.95	3	+	1	Org. C abundance, N isotopes, subsurface temperature	Ivanochko et al., 2005; Huguet et al., 2006
	P178-15P	11.96	44.30	1	+	1	Subsurface temperature	Tierney et al., 2015
	74KL	14.32	57.33	1	+	1	Subsurface temperature	Huguet et al., 2006
	93KL	23.58	64.22	2	+	1	Dust flux, authigenic uranium	Pourmand et al., 2004